Micro-structural and volumetric behaviour of bimodal artificial soils with aggregates

Vinícius de Oliveira Kühn[a]

[a] Universidade Federal do Oeste da Bahia, Centro das Ciências Exatas e Tecnologias, Barreiras, Bahia, 47808-021, Brazil, vinicius.kuhn@ufob.edu.br, 0000-0001-5648-4372, corresponding author

Bruna de Carvalho Faria Lima Lopes[b]

[b] University of Strathclyde, Civil and Environmental Engineering Department, Glasgow, G1 1XJ, Scotland, UK, bruna.lopes@strath.ac.uk, 0000-0001-7669-7236

Bernardo Caicedo[c]

[c] Universidad de Los Andes, Civil and Environmental Engineering Department, Bogotá, Bogotá, 111711, Colômbia, bcaicedo@uniandes.edu.co, 0000-0003-4344-0914

Manoel Porfírio Cordão Neto[d]

[d] Universidade de Brasília, Departamento de Engenharia Civil e Ambiental, Faculdade de Tecnologia, Brasília, DF, 70910-900, Brazil, porfirio@unb.br, 0000-0003-0618-4376

Highlights

- The methodology employed is capable of producing soil aggregates, which can be used in different proportions to obtain diverse structures;
- Artificial soils with aggregates and simple, non-mineralogical variability and controlled double porosity structures;
- The presence of aggregates in different proportions has a direct impact on soil's: plasticity; classification; compaction curve; retention curve; pore size distribution;
- Soil shrinking process associated with the drying of the macro and microstructure could be separated and related with its retention curve;
- Contribution to a better understanding of the role of aggregates on the microstructural and volumetric behaviour of bimodal soils.

Micro-structural and volumetric behaviour of bimodal artificial soils with aggregates

Vinícius de Oliveira Kühn[a]

[a] Universidade Federal do Oeste da Bahia, Centro das Ciências Exatas e Tecnologias, Barreiras, Bahia, 47808-021, Brazil, vinicius.kuhn@ufob.edu.br, 0000-0001-5648-4372, corresponding author

Bruna de Carvalho Faria Lima Lopes[b]

[b] University of Strathclyde, Civil and Environmental Engineering Department, Glasgow, G1 1XJ, Scotland, UK, bruna.lopes@strath.ac.uk, 0000-0001-7669-7236

Bernardo Caicedo[c]

[c] Universidad de Los Andes, Civil and Environmental Engineering Department, Bogotá, Bogotá, 111711, Colômbia, bcaicedo@uniandes.edu.co, 0000-0003-4344-0914

Manoel Porfírio Cordão Neto[d]

[d] Universidade de Brasília, Departamento de Engenharia Civil e Ambiental, Faculdade de Tecnologia, Brasília, DF, 70910-900, Brazil, porfirio@unb.br, 0000-0003-0618-4376

Abstract

Bimodal soils with aggregates present a complex micro-structural and volumetric behaviour. This occurs because they showcase several variables, such as mineralogical, different grain sizes and structures. The objective of this paper is to develop a methodology for producing soils with aggregates and simple, non-mineralogical variability and controlled double porosity. In this sense, aggregates using Kaolin were created to obtain bimodal samples. The aggregates produced with this methodology were stable in water and the bimodal samples were analysed by means of Mercury Intrusion Porosimetry (MIP), Scanning Electron Microscopy (SEM), Soil Water Retention Curve (SWRC) and analysis of the shrinking process. Results show that the presence of aggregates in different proportions has a direct impact on soil's: plasticity; classification; compaction curve; retention curve; as well as the pore size distribution (PSD), where micro and macro pores were observed. The shrinking and expansion analysis of the samples show that the presence of aggregates reduced both the expansive and shrinking potential. During the analysis of the shrinking process a fitting equation is presented to describe

the trend of volumetric strain of the samples, from which it was possible to separate the soil shrinking process associated with the drying of the macro and microstructure and its relationship with the retention curve. Therefore, this study contributes to a better understanding of the role of aggregates on the microstructural and volumetric behaviour of bimodal soils.

Keywords

Bimodal soil; aggregates; kaolin; soil structure; pore size distribution; volume change.

1. Introduction

Soil aggregates are secondary units which results from the binding of several soil particles (Unger and Mccalla, 1980). Soil aggregates play a major role in the formation of soil structure, which in turn influences the soil's behaviour. The most well-known example of aggregates influence in the behaviour of soils comes from the field of geological repositories for nuclear waste disposal, where highly compacted bentonite blocks and mixtures of bentonite powder, pellets and sand are often used as the main engineered barrier systems protecting the groundwater and soil from contamination (Alonso et al., 2011; Gens et al., 2011; Hoffmann et al., 2007; Lloret et al., 2003; Sánchez et al., 2016).

However, aggregates are also observed in other contexts. Delage (2009) in discussion with Tarantino and De Col (2008) noticed that the distribution of bimodal pores in compacted Kaolin samples produced in their study was linked to the aggregates formed during the process of wetting and sieving carried out during the samples' preparation stage. Bagherieh et al. (2009) and Foong et al. (2016) made similar observations using similar procedures. In these cases the aggregates formed by the wetting and sieving procedures are easily destroyed. That is, they do

not affect the geotechnical characteristics of the material, such as grain size distribution curve, compaction curve and Atterberg limits.

Additionally, aggregates can also be found in natural bimodal soils (Mitchell and Soga, 2005; Ng et al., 2017; Wang et al., 2019, 2020). Nevertheless, in tropical residual soils this is a remarkable characteristic. The weathering process of residual soils, particularly in well-drained regions, promote the formation of soils aggregates with a bimodal pore structure characterized by a large difference between the dominant micro and macro pores (Cordão Neto et al., 2018; Futai and Almeida, 2005; Guimarães, 2002; Lopes, 2016; Miguel and Bonder, 2012; Otálvaro et al., 2016, 2015; Queiroz, 2015; Silva, 2007, 2009), where the micro-porosity is formed by intra-aggregate spaces and macro-porosity is formed by inter-aggregate spaces (Alonso, 1998; Alonso et al., 1999; Mitchell and Soga, 2005; Romero, 2013; Romero and Simms, 2008). In these cases, the aggregates have a high stability in water due to the presence of cementing agents.

Despite previous studies on bimodal soils with aggregates, it is not clear what are their effects on the soil's engineering behaviour. Inspired by pioneering work of Burland (1990), Bressani (1990), Maccarini (1987) and others, that turned to the creation of artificial soils to help in the understanding of fundamental soil behaviour, this study purposes the development of a methodology for producing soils with simple structures, non-mineralogical variability and controlled double porosity with aggregates. Thus, the characteristics of the artificial bimodal soils produced are discussed in microstructural terms by means of Mercury Intrusion Porosimetry (MIP), Scanning Electron Microscopy (SEM), Soil Water Retention curve (SWRC) and shrinking process.

2. Methodology for producing soils with controlled double porosity

Kaolin was the material selected here to be used in the production of a control double porosity soil, as this material is basically composed of Kaolinite mineral; therefore it is a pure and classic material with non-mineralogical variability also adopted in several studies based on artificial soils (Alazaiza et al., 2016; Bagherieh et al., 2009; Foong et al., 2016; Lopes, 2016; Morgenstern and Tchalenko, 1967; Pedrotti and Tarantino, 2014; Sa'ari et al., 2015; Serna, 2012; Tarantino and De Col, 2008; Tarantino and Tombolato, 2005; Wheeler and Sivakumar, 1995; Yu et al., 2016).

The material used in the research was Kaolin 605-635, produced in Brazil. Some of the characteristics of the material include: liquid limit, w_L, of 54.6%, plastic limit, w_p, of 38.5%, resulting in a plastic index, PI, of 16.1%; specific gravity, Gs, of 2.54; the proportion of clay-sized (particle size smaller than 2 μm) is 55% while the proportion of silt-sized (particle size between 2 μm and 75 μm) is 45%; this soil is classified as high plasticity silt (MH) according to the Unified Soil Classification System (USCS).

The methodology proposed for the development of a control double porosity material is presented in Figure 1 and consists of: (i) initial compaction of Kaolin at high stress - in order to generate a soil with stable aggregates (Figure 1a); (ii) remoulding new samples by mixing a pre-determined proportion of the sample created in Figure 1a, properly oven dried and crushed, with a proportion of the original supplied Kaolin (Figure 1b); (iii) new compaction of samples produced in Figure 1b at a new moisture content (Figure 1c). This methodology is described in detail in the following sections.

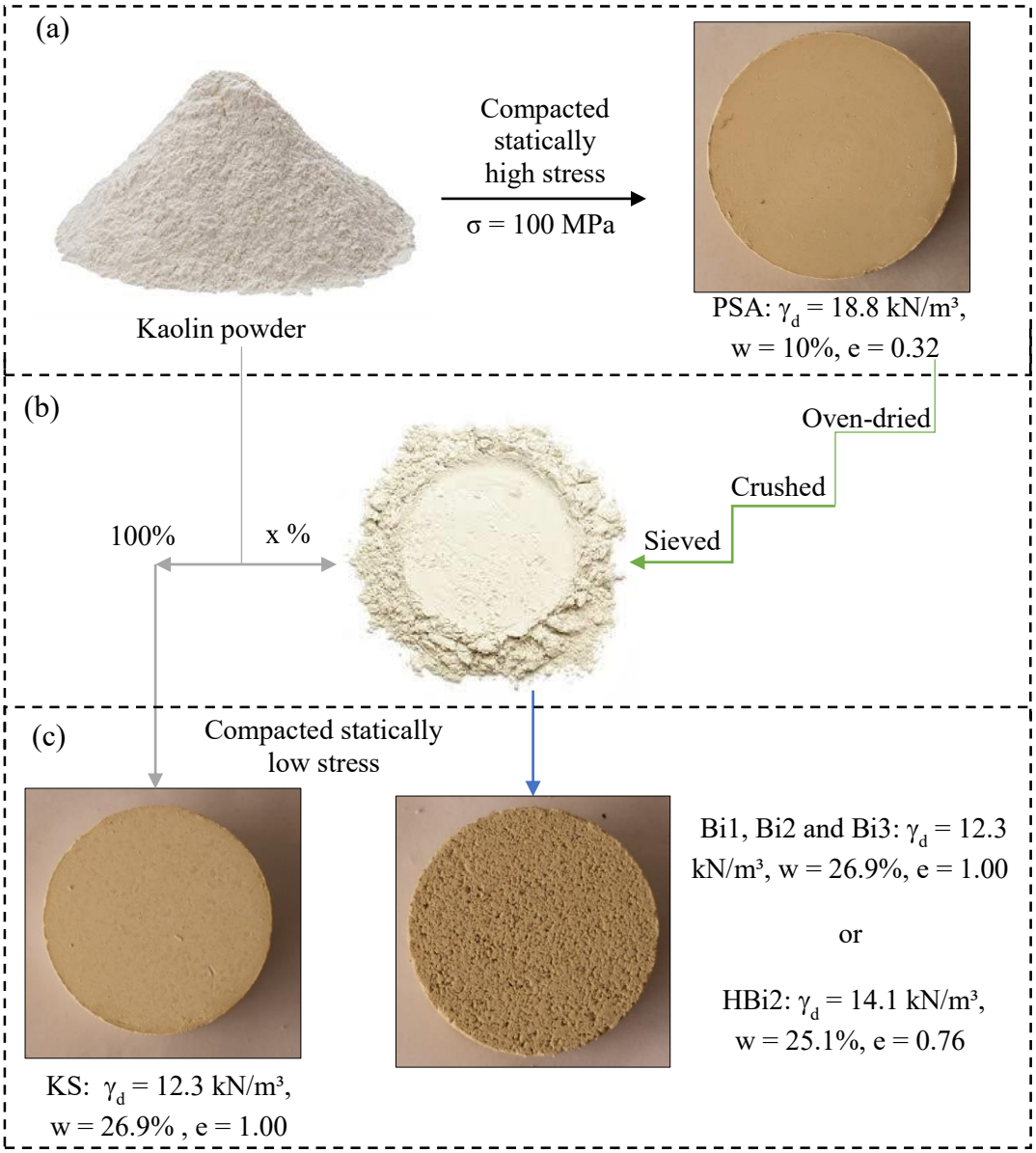

Figure 1 – Methodology for preparing bimodal samples: (a) high pressure compaction stage; (b) mixing step in different aggregate proportions; (c) low pressure compaction to obtain bimodal samples.

2.1 Preparation and characterization of artificial aggregates

As a starting point for obtaining artificial aggregates, compaction tests were performed using Standard Proctor and Mini Proctor (Villibor and Nogami, 2009) methodologies. The Kaolin powder was moistened and left to equilibrate for at least 24 hours before compaction. Figure 2a shows the compaction curves generated by these two methodologies; it can be observed a

good agreement between the compaction curves obtained with the Standard Proctor's energy and the Mini Proctor test, which highlights the validity of the Mini Proctor test.

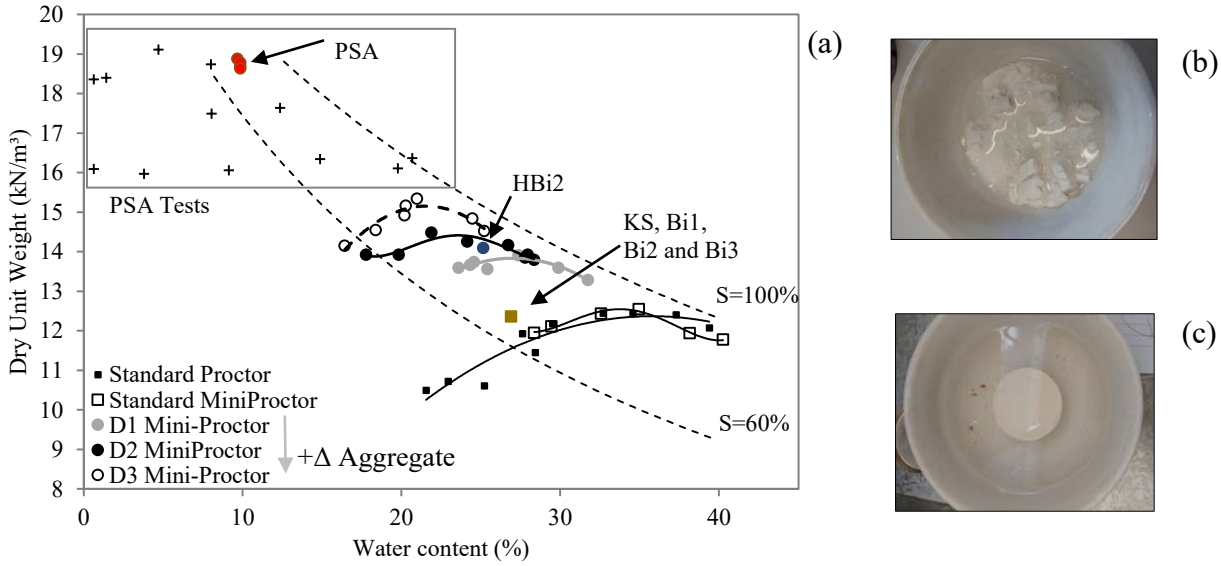

Figure 2 – (a) Compaction curves and stability tests to achieve stable microstructure; (b) unstable sample when submerged in water; (c) stable sample when submerged in water.

For the sake of producing artificial soils with controlled aggregate content, it is appropriate that the aggregates are stable when the material is immersed in water. This ensures that the aggregates remained in the samples at other preparation stages. Thus, after compaction, the stability of the samples was inspected by means of crumb tests (ASTM D6572, 2000), where samples were kept immersed in water for 12 hours, double the recommended by the standard. This test provides a simple and quick method for identifying dispersive clayey soil. Several crumb tests were performed on specimens coming from static compaction at different stress levels (20, 40, 50, 100 MPa) and water contents (1%, 3%, 5%, 8%, 10%, 15%, 20%).

The strain rate of 1.2 mm/min was applied. This was similar to that used by other authors in the literature (Rahardjo et al., 2004; Venkatarama Reddy and Jagadish, 1993; Wheeler and

130 Sivakumar, 1995). However, in the case under study, the sample was kept under the final load
131 for longer (30min) once the desired void ratio and stress level were reached. This decision was
132 a precaution made because the stress applied here (100 MPa) is much greater than the
133 conventional stress usually targeted. A time of 30 min was an extra measure used to ensure the
134 stress and water content distribution within the sample were homogeneous or in the very least
135 quasi-homogeneous, i.e., the excess pore-water pressure generated by the application of the
136 load dissipated before load was released. In the event that the excess pore-water pressure does
137 not dissipate before load was released an increase in sample volume, hence void ratio, should
138 be observed. No significant changes in the sample volume after the compaction stage were
139 observed (comparing the final void ratio obtained with the targeted void ratio, standard
140 deviation of 0.01 and coefficient of variation of 4.4%).

141

142 The points in Figure 2a represented by cross symbols show non-stable samples (Figure 2b)
143 while red circle points show the results of stable samples (Figure 2c) that were compacted
144 under 100 MPa at 10% of water content. This compaction produced samples that were stable
145 when immersed in water, here called Parent Sample of Aggregate (PSA), these samples had a
146 dry unit weight of 18.8 kN/m³, a degree of saturation of 80% and a void ratio of 0.32 (Figure
147 1a).

148

149 After obtaining a stable microstructure, the PSA samples were oven-dried at 105ºC (Figure
150 1b). In this temperature range there is no significant change in the kaolinite mineral (Caballero
151 et al., 2019; Carneiro et al., 2003; Cheng et al., 2019). The oven-dried, crushed and sieved
152 (sieve #10 – 2mm) material obtained from PSA samples are considered here the source of
153 aggregates; and for this reason the word aggregates is here used as synonym for the material

154 produced (PSA dried, crushed and sieved). Then, the material obtained was mixed with the
155 originally supplied Kaolin powder in different proportions (Figure 1b). Three aggregate
156 dosages were used. Dosage 1 had 100% of the mixed material passing through the 0.6 mm
157 sieve, 80% through the 0.2 mm sieve and 60% through the 0.075 mm sieve. Dosage 2 reflected
158 the grain size distribution of a bimodal soil provided by Otálvaro et al. (2015) without
159 dispersant (100% passing through the 0.6 mm sieve, 57.8% through the 0.2 mm sieve and
160 37.5% through the 0.075 mm sieve). Finally, dosage 3 had 40% of the mixed material passing
161 through the 0.2 mm sieve and 20% through the 0.075 mm sieve. That is, dosage 1 had the
162 lowest percentage of aggregate (40%) distributed between fine and medium sand-sized
163 diameters, dosage 3 had a higher aggregate content (80%) and dosage 2 intermediate aggregate
164 content (62.5%). That is, aggregate content is the amount of dried, crushed and sieved PSA
165 sample material used in each dosage.

166

167 The grain size distribution curves of kaolin samples, with and without dispersant, with different
168 aggregate contents are shown in Figure 3a and b, respectively. These graphs show a prominent
169 difference of the grain size distribution curve of the Kaolin with aggregate when determined
170 with and without dispersant. The grain size distribution curve of pure kaolin (dosage 0), without
171 dispersant, shows no material of the size that conventionally characterises clay-sized particles;
172 and stabilization of the curve in a diameter of 0.004 mm (Figure 3b). A higher percentage of
173 clay-sized is observed in the grain size distribution curve of the same specimen (dosage 0) with
174 dispersant (Figure 3a). This observation can be related to the effect of agglomeration and
175 flocculation of clay-sized particles. This occurs due to electrostatic forces between the particles
176 when immersed in an aqueous medium without a chemical dispersing agent, since this sample
177 does not have aggregates.

178

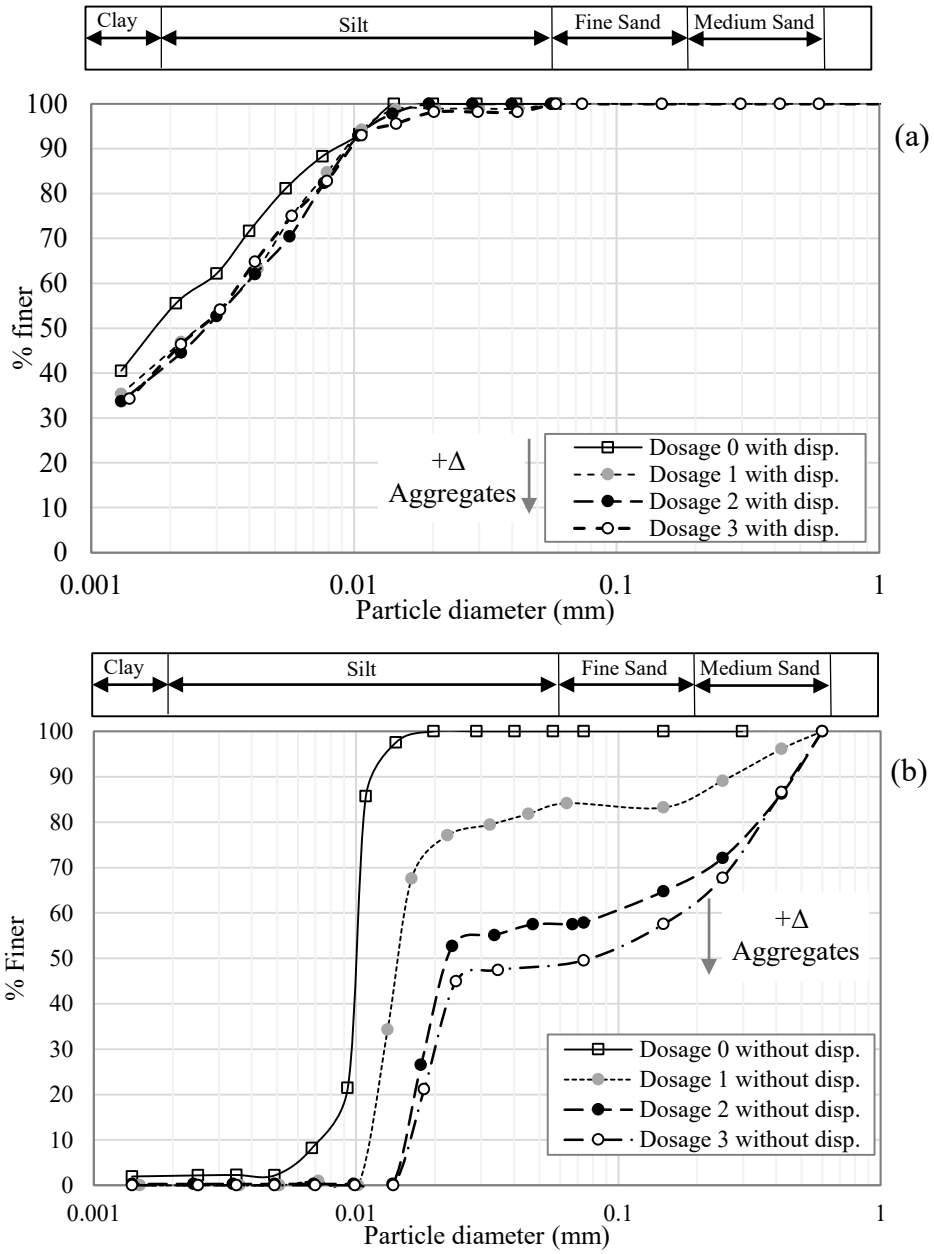

Figure 3 – Particle size distribution of Kaolin: (a) with dispersant; (b) without dispersant.

As the aggregate content increases, there was a tendency for the curves without dispersant to move to the right of the pure kaolin curve (dosage 0). That is, dosage 3 in the graph without dispersant showed a larger sand-sized diameter compared to dosage 2, followed by dosage 1. It is also apparent that the dispersant was able to eliminate the majority of aggregates. However, when comparing the grain size distribution, determined with dispersant, of pure Kaolin and Kaolin with aggregates, it is observed that some of the aggregates created in the Kaolin with

aggregates samples were not completely wiped out. Perhaps the dispersing agent was not enough to eliminate all aggregates formed in the initial compaction stage.

Atterberg limit tests were performed on all samples according to ASTM D4318 (2017). The mixing prior to the liquid limit test was performed for 30 min. The plastic limit test was carried out after the liquid limit test. The results are shown in Figure 4. Since the presence of aggregate changed the soil consistency, it was observed that the increase in aggregates content generated a decrease in the liquid limit and plasticity index (Figure 4a). Consequently, there was a modification on the soil classification from MH to ML (USCS). Extrapolating the trend observed in these three aggregate levels (Figure 4b), for a high aggregate content, there is convergence between w_L and w_p lines, which results in the complete loss of the plasticity index, similar to that observed in granular soils. Although the materials have the same mineralogy, the presence of aggregate reduced the specific surface of the particles, hence reducing their plasticity.

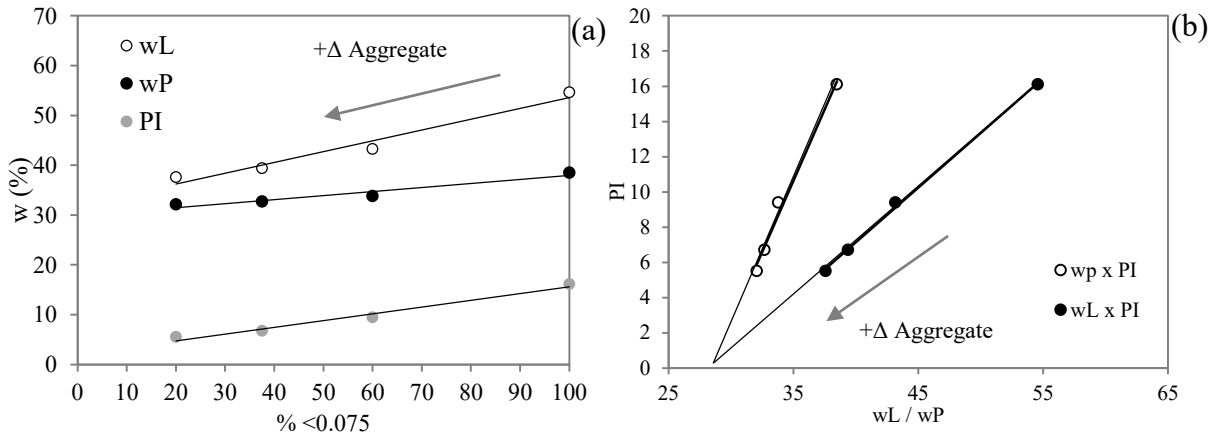

Figure 4 – Kaolin and Kaolin with aggregates: (a) Relationship between aggregate proportions and Atterberg limits; (b) Relationship between Atterberg limits and plasticity index.

Similar considerations were made by Sridharan et al. (1988) and Sridharan and Prakash (1998), who observed that the structure formed between particles affected the liquid limit. Along the same lines, Fearon and Coop (2000) observed an increase of the liquid limit and the plasticity index associated with the reconstitution of the sample and also with the energy and process of reconstitution. The authors observed significant differences between the Atterberg limits obtained depending on the method of reconstitution used: the standard procedure of hand mixing; passing the sample through a mixer; or passing it several times in a mincer. The observed tendency is an increase in the Atterberg limits with an increase in the energy use to reconstitute the samples. Similar to the tendency observed in this study, where an increase in aggregate content, which is the opposite to reconstitution, implicated in a decrease in the soil plasticity.

Regarding the compaction curves, it was noticed that the presence of kaolin aggregates generated a significant change in the compaction curve, with a decrease in the optimum water content and an increase in the dry unit weight (Figure 2a). Additionally, the shape of the compaction curve has narrowed with the increase of aggregate content.

2.2 Compaction of bimodal samples

These mixtures previously described (Figure 3) were used to obtain the compacted bimodal samples by means of static compaction at low stress. Two samples were produced from Dosage 2: (a) A sample compacted at a low energy to approach the dry branch of the compaction curve without aggregates (Figure 2a). The water content of this sample was w = 26.9% and the dry unit weight γ_d = 12.3 kN/m^3. This sample is herein referred to as Bimodal sample (Bi2); (b) A

sample with aggregates produced with water content of 25.1% and dry unit weight of γ_d=14.1 kN/m^3 (Figure 2a). This sample is herein referred to as High energy Bimodal sample (HBi2).

Two samples, compacted under the same water content and dry unit weight of Bi2, were produced from Dosage 1 and 3, herein named Bi1 and Bi3 respectively (Figure 2a). Another sample also compacted under the same water content and dry unit weight of Bi2, but now produced out of only Kaolin, i.e., without the presence of aggregates, is denoted here as Kaolin Sample (KS). Thus, four samples produced from different dosage mixtures were created, compacted under the same water content and dry unit weight. In ascending order of aggregate content, they are: KS, Bi1, Bi2 and Bi3. Table 1 summarizes the origin and compaction conditions of the samples produced.

Sample	Origin	w (%)	γ_d (kN/m³)	e
PSA	Pure Kaolin	10.0	18.8	0.32
KS	Pure Kaolin	26.9	12.3	1.00
Bi1	PSA and Pure Kaolin dosage 1	26.9	12.3	1.00
Bi2	PSA and Pure Kaolin dosage 2	26.9	12.3	1.00
HBi2	PSA and Pure Kaolin dosage 2	25.1	14.1	0.76
Bi3	PSA and Pure Kaolin dosage 3	26.9	12.3	1.00

Table 1 - Summary of origin and sample´s compaction conditions.

In order to prepare the samples for compaction, this procedure was followed: The kaolin material (Pure Kaolin – dosage 0; or a mixture of Pure Kaolin with PSA dried, crushed and sieve – dosage 1-3) was moistened using distilled water. After that the moistened material was sieved (sieve #10 – 2mm). The sieved material was stored in plastic bags for at least 24 hours before compaction. Finally, the material was moulded and statically compacted at strain rates

252 of 1.2 mm/min until the defined dry unit weight was reached. Samples were extruded using a
253 dummy cylinder head. The standard deviation of the moisture content obtained for Bi and PSA
254 samples was 0.31 and 0.34 respectively, while the standard deviation for the dry unit weight
255 for Bi and PSA samples was 0.16 and 0.18 respectively.

256

257 **2.3 Procedures for assessing the micro-structural behaviour**

258 Parent Sample of Aggregate (PSA), Bimodal Samples (Bi1, Bi2 and Bi3), High Energy
259 Bimodal Sample (HBi2) and Kaolin Sample (KS) were characterized by their SWRC,
260 shrinkage curve and PSD, complemented with SEM images.

261

262 The PSD of the specimens was measured using the MIP and qualitatively assessed by means
263 of SEM images. Before carrying out the tests, specimens of 1 cm^3 in volume were prepared
264 following freeze-drying. This technique consisted in applying rapid freezing with immersion
265 in liquid nitrogen and then placing the specimen in a lyophilizer applying a pressure of 5 Pa
266 and temperature of -50 °C for 24 hours. This methodology is reported by Delage and Lefebvre
267 (1984) and Mitchell and Soga (2005) as the least disturbing freeze-drying procedure.

268

269 The SWRC was measured for the entire suction range using two testing procedures. To
270 determine the SWRC, axis translation tests for suctions up to 500 kPa and dewpoint
271 psychrometer (WP4C) for suctions above 500 kPa were used. Although the axis translation
272 technique imposes matric suctions, and WP4C measures total suctions, both measurements
273 showed a good agreement which allows the determination of one SWRC in terms of matric
274 suction, in the same way performed by Tarantino and De Col (2008).

Fredlund (2002) integrated the shrinkage curve obtained by physical indexes (e versus w) with the SWRC (w versus s), and noted that the shape of the shrinkage curve in terms of suction is similar to the shape of the unimodal SWRC. Similar fittings of the shrinking process were also performed by Peng and Horn (2005) and Cornelis et al. (2006). To obtain the shrinkage curve (relationship between void ratio and water content), a caliper, an analytical balance and an oven were used. The water content obtained was converted into suction using Durner´s fitting (1994) from a previously determined SWRC. This procedure is similar to that adopted by Otálvaro et al. (2016). Both, in the tests carried out for determining the SWRC, and in the tests performed for determining the shrinkage curves, after compaction, specimens were wetted until the capillarity saturation was reached and then they were submitted to drying paths. The capillary saturation was performed by placing a porous stone and filter paper at the base of the sample then the assembly was placed in an airtight container. Water added to the container comes into contact with the porous stone and the soil absorbs water by capillarity upwards. This procedure is similar to that adopted by Hird and Bolton (2017).

3. Results and discussions

3.1 Pore Size Distribution and Scanning Electron Microscopy

The results of the MIP tests were adjusted using an equation proposed by Durner (1994) and adapted by Lopes et al. (2014) for bimodal soils. Figure 5a presents the results of the MIP tests obtained for KS, Bi1, Bi2 and Bi3 samples (all of these were compacted under the same conditions of water content and dry unit weight, having different aggregate content). The PSD shown in Figure 5b is obtained by deriving the cumulative intrusion curves, as suggested by Romero (1999). Figure 5c and d shows a comparative of samples prepared with the same

298 aggregate content but under different compaction conditions (water content, dry unit weight
299 and void ratio).

300

301 The bimodal PSD of Bi2 and Bi3 samples observed in Figure 5b is unquestionable. The
302 difference between the sizes of the dominant micro (≈ 0.1μm) and macro pores (≈ 100μm) in
303 this samples reached 3 orders of magnitude. As the aggregate content increased, there was an
304 increase in the size of the macro pores. On the other hand, in the micro pores range a higher
305 frequency of pore diameters is observed, meanwhile the higher is the aggregate content the
306 smaller are the diameters of micro pores noticed. In other words, it can be observed an increase
307 in the bimodality of the samples as aggregate content rises. However, from Bi2 to Bi3 sample,
308 despite an increase in the aggregate content, little change was observed in the macro pores
309 region.

310

311 It is important to note that previous researches showed little or no change on the micro pore
312 after compaction and oedometer tests (Cordão Neto et al., 2018; Otálvaro et al., 2016; Wang
313 et al., 2020). The difference observed in this paper in the micro-pores range is due to the stress
314 level applied to PSA samples (100 MPa), that is far above the conventionally applied values
315 found in the literature. Additionally, samples with the same aggregate content but compacted
316 under different conventional energy levels (Bi2 and HBi2) show the same micro pore size. The
317 increase in compaction energy in this case leads to a decrease only at the macro-pore level
318 (Figure 5d), as observed in the aforementioned researches.

319

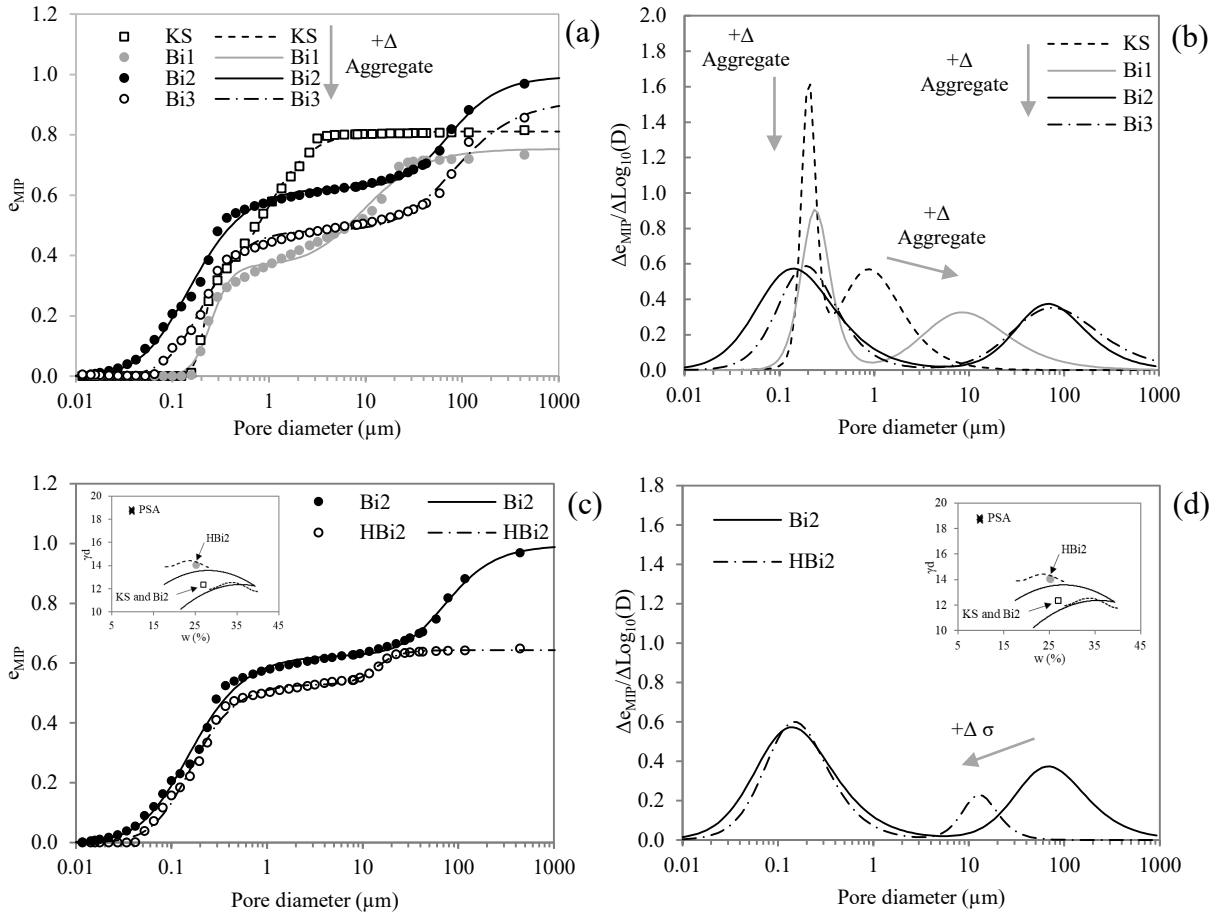

Figure 5 – MIP tests of KS, Bi1, Bi2 and Bi3: (a) Intrusion curve; (b) PSD; MIP tests of Bi2 and HBi2: (c) Intrusion curve; (d) PSD.

The KS sample, which is composed of only pure Kaolin and was compacted in the same conditions (w = 26.9%, γ_d = 12.3 kN/m³) as Bi2, presents slightly bimodal behaviour where the difference between macro and micro pore sizes are not significant. Similar results have been observed by other authors (Sivakumar et al., 2010; Tarantino and De Col, 2008; Thom et al., 2007) in samples of compacted kaolin, and in samples of reconstituted kaolin at low vertical stress levels (Lopes, 2016). At the same time, intermediate pore sizes (in the range of 2.0 μm) observed in the KS sample are not present in the Bi2 sample.

The void ratios obtained by the MIP are smaller than the void ratios of the samples. The difference is 0.06 for Bi2, 0.11 for HBi2, 0.26 for KS, 0.21 for Bi3 and 0.32 for Bi1 sample.

335 According to Romero and Simms (2008), this problem is usually observed in clayey soils due
336 to the difficulty of the mercury in filling the smaller pores of the soil, non-intruded porosity.
337 According to the authors, the differences between the void ratios can also be attributed to: (i)
338 isolated pores surrounded by solids which are not intruded; (ii) some pores which are accessible
339 only through smaller pores, i.e. they are not detected until smaller pores are penetrated,
340 restricted porosity; (iii) the minimum pressure of the apparatus limits the smallest pore size to
341 be detected, porosity not detected. Other researches have reported differences between the
342 voids ratios obtained by MIP in relation to the void ratios of the samples (Cordão Neto et al.,
343 2018; Lopes, 2016; Pedrotti, 2016). It is worth mentioning that some authors have also
344 observed the occurrence of compression on soft samples during the mercury intrusion phase
345 (Penumadu and Dean, 2000).

346

347 SEM imaging is a complementary method for analysing the soil's microstructure. Figure 6 and
348 Figure 7 show SEM images of the bimodal Bi2 and HBi2 samples at different scales. From
349 these figures, it is possible to recognise that Bi2 sample sustain a bimodal pore structures while
350 the increase in the compaction energy is responsible for the reduction of the macro pores
351 observed on the HBi2 sample (Figure 7). Considering the images of the HBi2 sample at the
352 larger scale, it is possible to notice that the aggregates formed over the high-energy compaction
353 have a predominantly face-to-face structure (Figure 7). Qualitatively, the images correspond to
354 the dominant pore sizes presented in Figure 5. These SEM images validate the proposed
355 methodology for preparing bimodal samples adopted in the research.

356

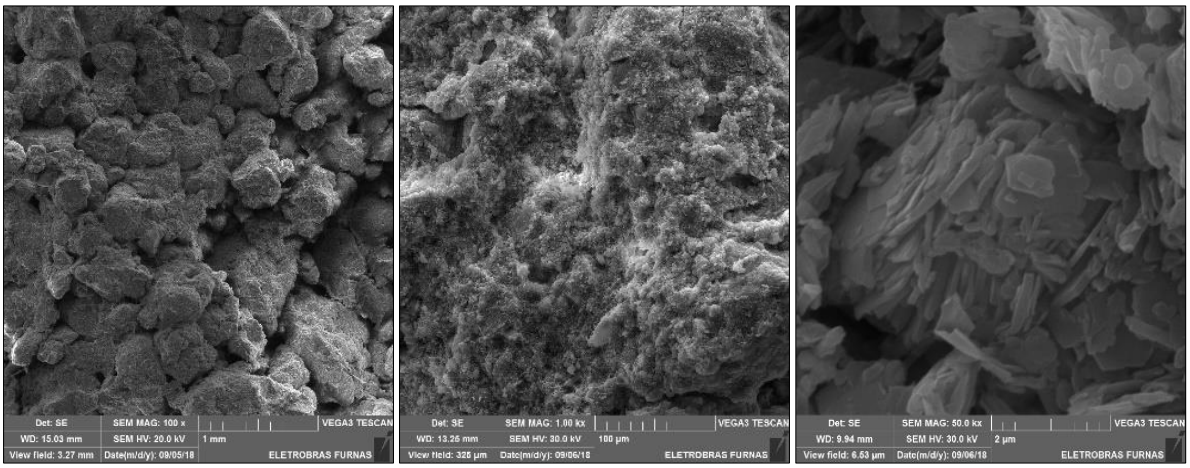

Figure 6 – SEM images of Bi2 sample.

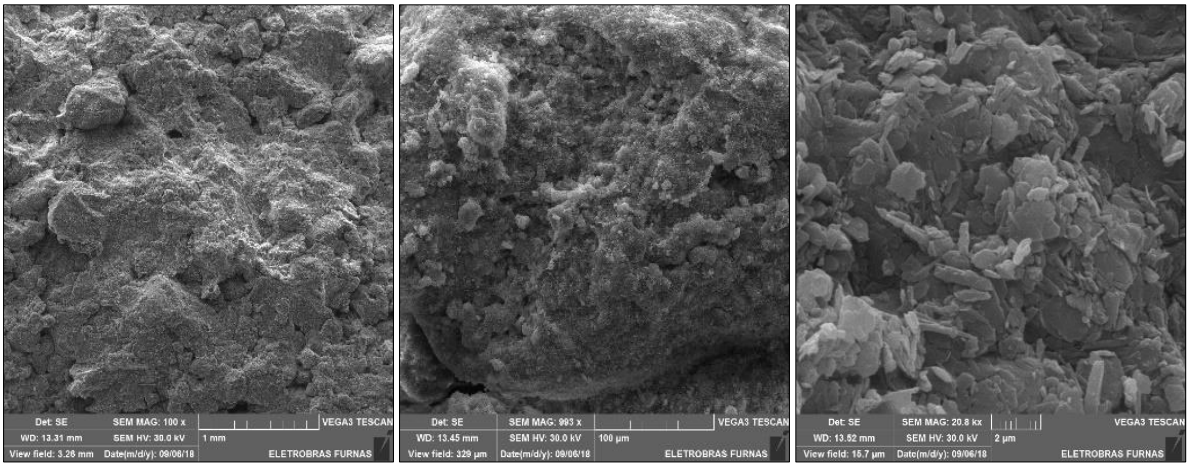

Figure 7 – SEM images of HBi2 sample.

3.2 Soil Water Retention Curves

The SWRC, expressed in terms of water ratio ($e_w = V_w / V_s$), was adjusted using Durner's (1994) equation, which is a generalization of the van Genutchen's equation (1980) for multimodal soils. For bimodal soils:

$$e_w = \frac{e_w^L}{\left[1+(a_L.s)^{n_L}\right]^{1-1/n_L}} + \frac{e_w^S}{\left[1+(a_S.s)^{n_s}\right]^{1-1/n_s}} \qquad \text{(Eq. 1)}$$

where: *a* and *n* are fitting parameters, *s* is suction, L and s subscriptions stand for large and small respectively.

Table 2 presents the fitting parameters used to adjust the SWRC. Figure 8a shows the SWRC of PSA, KS, Bi2 and HBi2, while Figure 8b shows the SWRC of KS, Bi1, Bi2 and Bi3 (in this last figure all samples were compacted under the same condition of water content and dry unit weight, having different aggregate contents).

SWRC Fitting							Shrinkage curve Fitting						
	PSA	**KS**	**Bi1**	**Bi2**	**Bi3**	**HBi2**		**PSA**	**KS**	**Bi1**	**Bi2**	**Bi3**	**HBi2**
R^2	0.99	0.99	1.00	0.99	0.99	1.00	R^2	0.99	0.99	0.99	0.99	0.99	1.00
e_w^L	0.00	0.78	0.42	0.32	0.45	0.29	Δe^L	0.00	0.23	0.06	0.11	0.03	0.04
a_L	0.000	0.140	0.084	0.049	0.115	0.023	b_L	0.000	0.084	0.051	0.051	0.109	0.013
n_L	1.00	1.31	2.36	10.12	7.86	1.81	p_L	1.00	1.73	7.69	7.35	14.45	9.79
e_w^S	0.43	0.79	0.85	0.68	0.72	0.60	Δe^S	0.06	0.15	0.09	0.07	0.11	0.06
a_S	0.001	0.002	0.002	0.001	0.002	0.001	b_S	0.002	0.003	0.003	0.002	0.002	0.003
n_S	1.69	3.26	1.76	2.04	1.71	1.90	p_S	2.16	5.03	3.16	2.72	3.52	2.69
e_{wsat}	0.43	1.57	1.28	0.99	1.17	0.89	e_{res}	0.37	0.98	0.91	0.94	0.86	0.72
							e_{sat}	0.44	1.41	1.06	1.119	1.01	0.82

Table 2 – Fitting Parameter of SWRC and shrinkage curves.

The significant difference between the SWRC of the KS and Bi2 samples confirms that the proposed methodology is adequate for the creation of bimodal soils. Although both samples, KS and Bi2, were compacted under the same conditions of water content and void ratio, the presence of aggregates in Bi2 was determinant to produce a bimodal structure. In fact, for Bi2 sample (Figure 8a), water starts to drain out of the macro pores at a suction of 15 kPa and from the micro pores at 1500 kPa. On the other hand, in the KS sample it is not possible to clearly identify the level in which the draining within the macro pores ends and the draining amongst the micro pores begins (Figure 8a). In contrast, the higher density imposed on the compaction of the HBi2 sample reduced the size of the macro pores and the bimodal shape of the SWRC

386 is less evident. While the SWRC of the PSA sample presents unimodal characteristics due to
387 the high energy applied during its constitution (100 MPa).

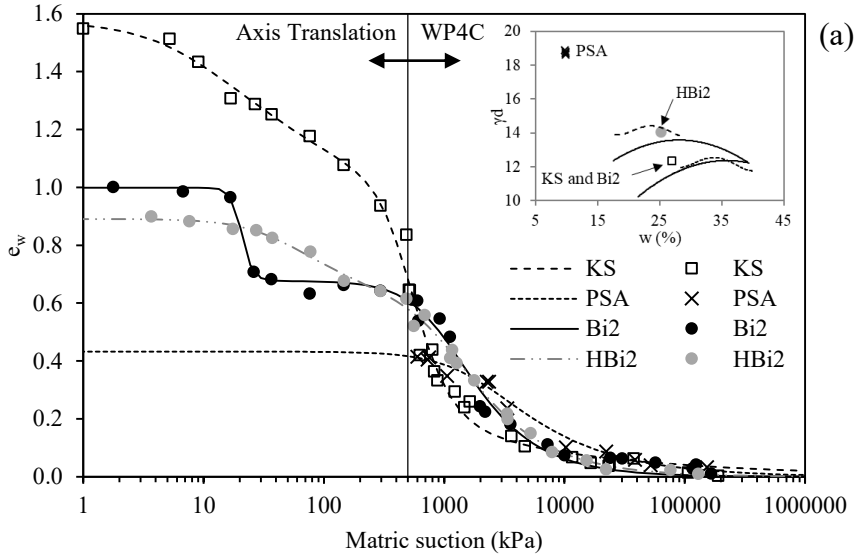

388

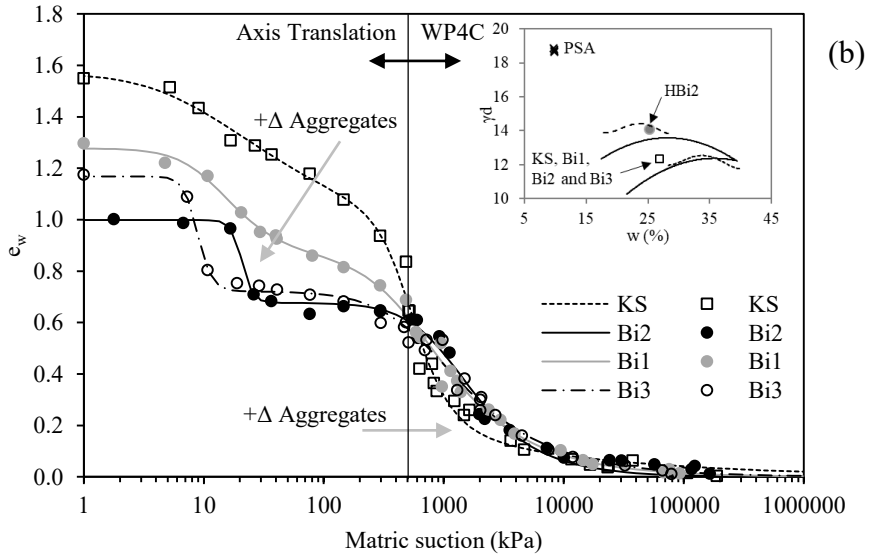

389

390 Figure 8 – Soil Water Retention Curve: (a) PSA, KS, Bi2 and HBi2; (b) KS, Bi1, Bi2 and
391 Bi3.

392

393 The SWRCs show that the origin of the double porosity of the samples is considerably
394 influenced by the presence of aggregates (Figure 8b). The trend is that the distance between
395 macro and micro pores increases with the rise in the aggregate content, which is highlighted by
396 the intermediate plateau of the SWRC of samples with aggregates. The suction value related to

397 the air entry value of the macro pores show a decrease with the increase in aggregate content,
398 and the micro pores a decrease in size caused by primary compaction process.

399

400 As the void ratio of the samples after the compaction process is the same (the only thing that
401 differentiates the samples is the aggregate content), it is understood that the decrease in the
402 diameters of micro pores with primary compaction and the formation of aggregates generated
403 an increase in the macro pores of the samples. In other words, a redistribution of the pores
404 within the samples took place because the particles are now in an aggregated form. However,
405 it is important to note that the presence of aggregates decreased the expansive potential of the
406 samples, which also affects the redistribution of pores during the wetting and drying processes.
407 The issues related to volumetric variation will be dealt with in the following section.

408

409 **3.3 Volumetric behaviour and proposed shrinkage equation**

410 The volumetric behaviour of the samples was evaluated during the wetting and drying process.
411 Table 3 presents volumetric deformations, considering: the wetting phase, the drying phase and
412 the total deformation.

413

Sample	$e_{initial}$	e_{sat}	$\varepsilon_{wetting}$ (%)	e_{final}	ε_{drying} (%)*	ε_{total} (%)**
PSA	0.31	0.49	-13.5	0.37	7.8	-4.7
KS	1.02	1.33	-15.3	0.99	14.4	1.3
Bi1	1.01	1.06	-2.9	0.90	7.9	5.2
Bi2	1.01	1.10	-4.5	0.94	7.6	3.5
Bi3	1.00	1.00	-0.3	0.85	7.6	7.4
HBi2	0.75	0.82	-3.7	0.72	5.5	2.0

414 *the initial void ratio considered is the e_{sat}, **the initial void ratio considered is $e_{initial}$.

415 Table 3 – Void ratios and volumetric deformations of samples subjected to wetting and drying.

The PSA and KS samples, when compared to the samples with aggregates (Bi1, Bi2, Bi3 and HBi2) present higher expansion once saturated while presenting higher skrinkage when drying (Table 3). This observation shows that (i) the presence of aggregates decreases the expansion and shrinkage, for wetting and drying respectively. And these reductions are also related with (ii) the reduction in the plasticity of Bi samples and eventually with (iii) the reduction on the specific surface which in turn is a product of the formation of aggregates. When comparing Bi2 and HBi2 samples (Table 3), the increase of energy during the secondary compaction process led to a reduction of the expansion potential of the HBi2 sample.

In terms of total volumetric deformation, it is observed that the PSA sample showed more expansion than shrinkage, which resulted in a negative total volumetric deformation, and non-recoverable deformations. The opposite is observed in the other samples, in which the final total deformation is positive, indicating more shrinkage than expansion, which is related to the structure formed during the compaction processes.

Thus, in samples with aggregates, during wetting, there is an expansion of aggregates generating a closure of macro pores with a slight variation in the total volume of the sample. The same occurs during the drying process, with shrinkage of aggregates and small variation in total volume. This behaviour agrees with the analyses carried out by Romero (2013), which demonstrated that the expansion of the microstructure by wetting can alter the macrostructure, that is, there is an interaction between the different levels of structure (invasion or retraction of macro pores due to expansion or shrinkage of micro pores). The observations here reported are also in line with Alonso et al. (1999), who showed a trend of volumetric variation caused by the expansion of the microstructure.

Regarding the shrinkage curves of the samples (Figure 9), a fitting equation based on Durner (1994)'s proposal, with the intention of describing the shrinkage path of the soils, is suggested for relating the void ratio of the sample to the suction during the drying path.

$$e = \frac{\Delta e^{L}}{\left[1+(b_{L}.s)^{p_{L}}\right]^{1-1p_{L}}} + \frac{\Delta e^{S}}{\left[1+(b_{S}.s)^{p_{s}}\right]^{1-1/p_{s}}} + e_{res} \qquad \text{(Eq. 2)}$$

where b and p are fitting parameters, e_{res} is the residual void ratio when reaching the non-deformable state on drying, Δe^{L} and Δe^{S} represent the variation of voids ratio provided by the drying of the macro and micro pores, respectively.

Table 2 shows the fitting parameters used to adjust the shrinkage curve. It is important to point out that the parameter a_L (from SWRC) are close to the values of the fitting parameter b_L on the corresponding shrinkage curve. The same observation could be drawn for the parameters related to the drainage of the micro pores (a_s) and starting of the shrinkage, as a result of the drying of the micro pores (b_s). The residual void ratio (e_{res}) is that obtained after the shrinking limit of the soil, in which there is no more volumetric variation. Finally, the sum of the residual void ratio (e_{res}) with the variation of the void ratio due to the shrinkage of the micro pores (Δe^{S}) and the variation of the void ratio due to the shrinkage of the macro pores (Δe^{L}) must be equal to the voids ratio of the saturated soil (e_{sat}).

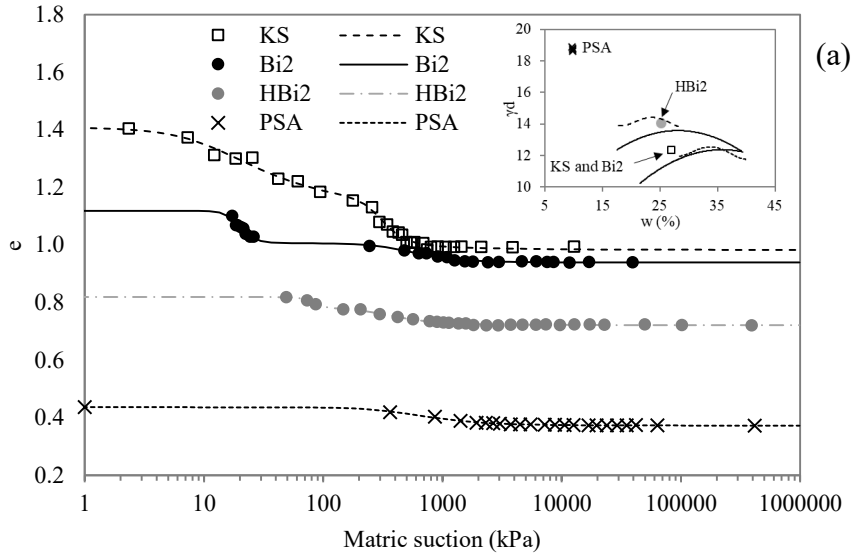

460

461

462 Figure 9 – Shrinkage curve of samples: (a) PSA, KS, Bi2 and HBi2; (b) KS, Bi1, Bi2 and
463 Bi3.

464

465 The shrinkage curve of the PSA sample is fitted unimodally. As a result, equation 2 is reduced
466 to two terms, as in the case of unimodal fittings one of the Δe becomes zero, and the fitting
467 parameters b and p related to this term become obsolete. The remaining samples are fitted with
468 the bimodal equation. In general, all fittings prove that the shrinkage fitting equation is quite
469 effective in reproducing the shrinkage paths during drying (R^2 ranging from 0.99 to 1.00).

470

471 The shrinking behaviour occurs at different ranges of suction and is directly related to drainage
472 of the macro and micro pores as represented by their SWRCs. Four shrinkage curves and their
473 respective SWRC are presented: PSA (Figure 10a), Bi2 (Figure 10b), KS (Figure 10c) and Bi3
474 (Figure 10d). Indeed, regarding the bimodal samples the shrinking begins with the drainage of
475 water from the macro pores and then continues with the drainage of the water from the micro
476 pores. For example, for Bi2 sample (Figure 10b), it is observed that between suction of 30 and
477 200 kPa there is no drainage of water from the pores and, therefore, in this range there is no
478 shrinking of the sample, as demonstrated by the experimental shrinkage data and corresponding
479 fitting curve (Figure 10b). Similar observations can be drawn for other bimodal samples. On
480 the other hand, the PSA sample characterised by unimodal SWRC shows shrinking beginning
481 on the same suction range where the pore drainage begins (Figure 10a).

482

483 In all cases, shrinking within the micro pores occurs approximately halfway up the drainage
484 section of the micro pores, until the samples reach a residual void ratio. This is due to the fact
485 that shrinking is motivated by the increase of suction hence decrease of water meniscus in the
486 soil. It appears that in the case under study, after half of the drainage of the micro pores, the
487 water will no longer be in its capillary form, it is now immobile - only present in the form of
488 meniscus, thus stopping soil shrinkage (Lu, 2016; Lu and Dong, 2017; Tuller and Or, 2005).

489

490 Based on the proposed fitting equation and the data presented in Table 2, it is possible to
491 separate the variation in voids ratio associated with the drainage of micro and macro pores
492 during the drying process, as well as to determine which suction values are thresholds
493 responsible for the process of shrinkage of the samples.

494

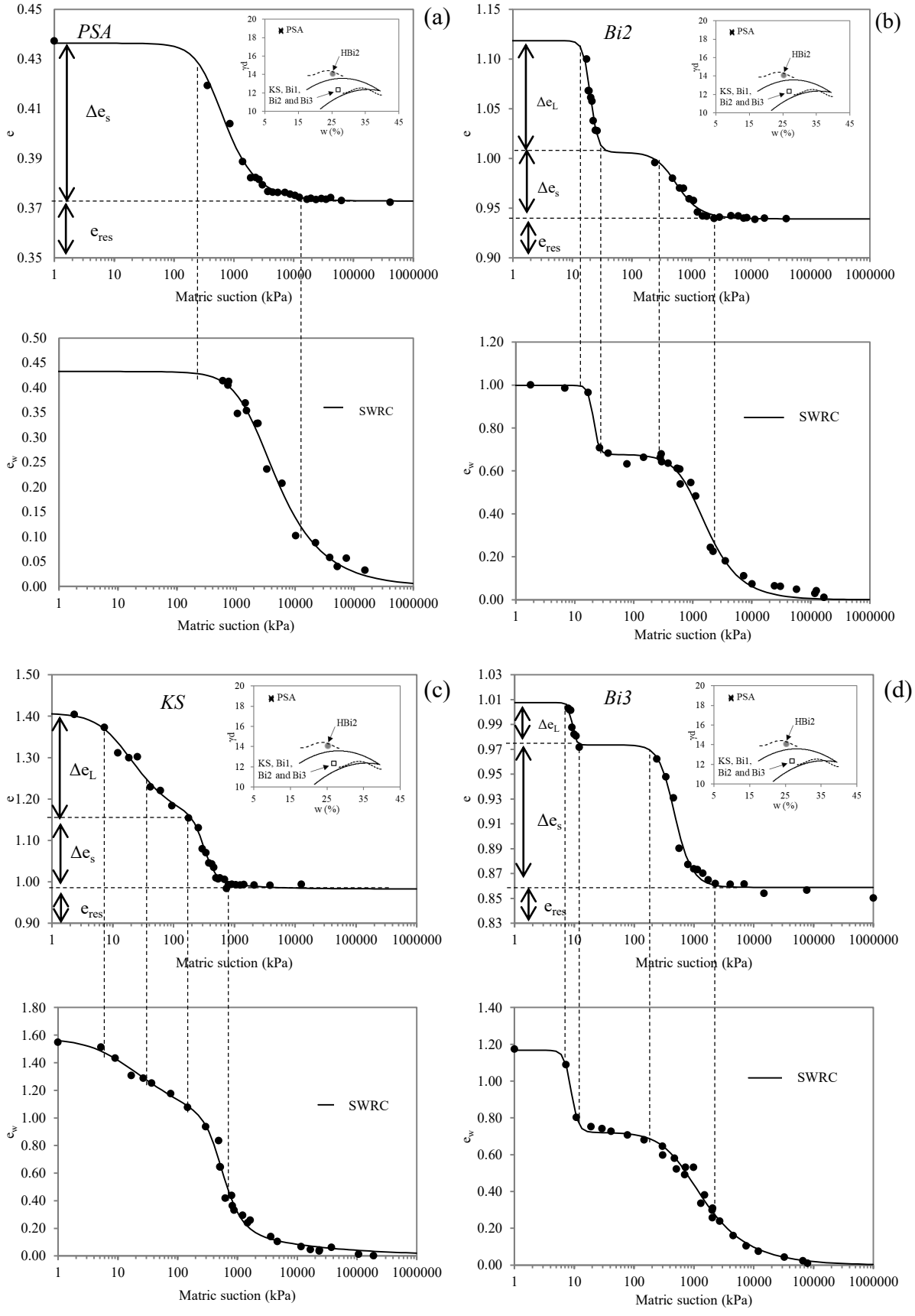

Figure 10 – (a) Shrinkage curves applied to proposed fitting equation, together with SWRC and interest points: (a) unimodal sample PSA; (b) bimodal sample Bi2; (c) KS; (d) Bi3.

4. Conclusions

Previous researches have recognised that the soil structure is one of the key soil elements that needs to be examined to allow for a fully comprehensive understanding of its behaviour. In the interest of contributing to a better understanding of the role of aggregates on the microstructural behaviour of bimodal soils, this paper described a new methodology for producing soils with simple - non-mineralogical variability and controlled double porosity - structures.

The methodology proposed consisted in creating aggregate by compacting Kaolin at high stresses (100MPa). The product of this sample was then oven-dried, crushed, sieved and mixed in different proportions with additional Kaolin powder to create samples with different aggregate content. Thus, four samples were produced and compacted under the same conditions of water content, dry unit weight and void ratio, having different aggregate contents (0, 40, 62.5 and 80%). An additional sample, with 62.5% aggregate content was compacted targeting lower water content and void ratio and higher dry unit weight.

The aggregates within the samples created were stable in water, which is crucial to ensures that aggregates remained in the samples at other preparation stages. This also allows to control the aggregates content and the double porosity. This stability was observed when comparing the grain size distribution of the different aggregate content samples without dispersant. Another important observation to be highlighted is that although the materials have the same mineralogy, the presence of aggregates reduced the specific surface of the particles, hence reducing their plasticity. This has also led to a decrease in expansivity with an increase in aggregate content. Additionally, the increase in aggregate content have also promoted change in the soil classification and compaction curve.

525 The samples created were assessed microstructurally by means of Soil Water Retention Curves
526 (SWRC) and Pore Size Distribution (PSD), as well as qualitatively by Scanning Electron
527 Microscopy (SEM) images. A relevant characteristic of the soils obtained with the proposed
528 methodology is the bimodality. The difference between the sizes of the dominant micro and
529 macro pores reached 3 orders of magnitude. It was observed that the increase in the size of
530 dominant macro pores is associated with the increase in aggregate content up to a point, since
531 no significant change in the dominant macro pores were observed between samples with
532 aggregate content of 62.5 and 80%. Furthermore, the increase in compaction density led to a
533 reduction in the difference between the size of dominant micro and macro pores together with
534 a slight change in the size of micro pores.

535

536 The microstructural behaviour of the bimodal soils was also studied through their shrinkage
537 curves. These curves showed that the presence of aggregates decreased the expansion and
538 shrinkage of the samples. Moreover, in terms of suction, the shrinkage curves show tendency
539 of shrinking similarly to the drainage observed in the SWRC. Based on these results, a fitting
540 equation based on the soils' volumetric strain behaviour was developed fitting successfully the
541 experimental shrinkage data.

542

543 Additionally, it is important to highlight that the methodology proposed for preparing bimodal
544 soils produces soils with aggregates and non-mineralogical complexity (i.e., macro pores and
545 aggregates are both made out of Kaolin material), which emphasises difference between micro
546 and macro structure. This characteristic could be extremely useful for differentiating the effect
547 of the soil microstructure on its macroscopic behaviour. The next stages of the research involve

548 assessing the hydro-mechanical characteristics of these artificial bimodal soils as well as the
549 effects that the double porosity caused on them.

550

551 ## Acknowledgements

552 The authors would like to thank the Geotechnics program of University of Brasília and Federal
553 University of Western Bahia for the support provided to carry out this research as well as
554 University of Los Andes and Eletrobrás Furnas. The authors would also like to acknowledge
555 the Brazilian research council, the National Council for Scientific and Technological
556 Development (CNPQ) for providing the funds for the acquisition of equipment used in this
557 research.

558

559 ## References

560 Alazaiza, M.Y.D., Ngien, S.K., Bob, M.M., Kamaruddin, S.A., Faizal Ishak, W.M., 2016.
561 Assessment of the behaviour of soil structure in double-porosity kaolin media using light
562 transmission visualization (LTV) method. Int. J. Geotech. Eng. 11, 316–320.
563 https://doi.org/10.1080/19386362.2016.1211370

564 Alonso, E.E., 1998. Modelling Expansive Soil Behaviour, in: Proceedings Of The Second
565 International Conference On Unsaturated Soils. p. 7625.

566 Alonso, E.E., Romero, E., Hoffmann, C., 2011. Hydromechanical behaviour of compacted
567 granular expansive mixtures: experimental and constitutive study. Géotechnique 61,
568 329–344. https://doi.org/10.1680/geot.2011.61.4.329

569 Alonso, E.E., Vaunat, J., Gens, A., 1999. Modelling the mechanical behaviour of expansive
570 clays. Eng. Geol. 54, 173–183. https://doi.org/10.1016/S0013-7952(99)00079-4

571 ASTM, 2017. D4318-17e1, Standard Test Methods for Liquid Limit, Plastic Limit, and
572 Plasticity Index of Soils. West Conshohocken, PA.

573 ASTM, 2000. D 6572-12 Standard Test Methods for Determining Dispersive Characteristics
574 of Clayey Soils by the Crumb Test. ASTM Int. 11, 3–6.

575 Bagherieh, A.R., Khalili, N., Habibagahi, G., Ghahramani, A., 2009. Drying response and
576 effective stress in a double porosity aggregated soil. Eng. Geol. 105, 44–50.
577 https://doi.org/10.1016/j.enggeo.2008.12.009

578 Bressani, L.A., 1990. Experimental properties of bonded soils. University of London.

579 Caballero, L.R., Paiva, M. das D.M., Fairbairn, E. de M.R., Toledo Filho, R.D., 2019.
580 Thermal, Mechanical and Microstructural Analysis of Metakaolin Based Geopolymers.
581 Mater. Res. 22, 1–8. https://doi.org/10.1590/1980-5373-mr-2018-0716

582 Carneiro, B.S., Angélica, R.S., Scheller, T., Castro, E.A.S. de, Neves, R.F., 2003.
583 Mineralogical and geochemical characterization of the hard kaolin from the Capim
584 region, Pará, northern Brazil (in portuguese). Cerâmica 49, 237–244.
585 https://doi.org/10.1590/s0366-69132003000400008

586 Cheng, Xing, Bu, Zhang, Piao, Huang, Xie, Wang, 2019. Dehydroxylation and Structural
587 Distortion of Kaolinite as a High-Temperature Sorbent in the Furnace. Minerals 9, 587.
588 https://doi.org/10.3390/min9100587

589 Cordão Neto, M.P., Hernández, O., Lorenzo Reinaldo, R., Borges, C., Caicedo, B., 2018.
590 Study of the relationship between hydro-mechanical soil behavior and microstructure of
591 a structured soil. Earth Sci. Res. J. 22, 91–101.
592 https://doi.org/10.15446/esrj.v22n2.65640

593 Cornelis, W.M., Corluy, J., Medina, H., Díaz, J., Hartmann, R., Van Meirvenne, M., Ruiz,

M.E., 2006. Measuring and modelling the soil shrinkage characteristic curve. Geoderma 137, 179–191. https://doi.org/10.1016/j.geoderma.2006.08.022

Delage, P., 2009. DISCUSSION: Compaction behaviour of clay. A. TARANTINO and E. DE COL (2008). Géotechnique 58 , No, 3, 199–213. Géotechnique 59, 75–77. https://doi.org/10.1680/geot.2008.59.1.75

Delage, P., Lefebvre, G., 1984. Study of the structure of a sensitive Champlain clay and of its evolution during consolidation. Can. Geotech. J. 21, 21–35. https://doi.org/10.1139/t84-003

Durner, W., 1994. Hydraulic conductivity estimation for soils with heterogeneous pore structure. Water Resour. Res. 30, 211–223. https://doi.org/10.1029/93WR02676

Fearon, R.E., Coop, M.R., 2000. Reconstitution: What makes an appropriate reference material? Geotechnique 50, 471–477. https://doi.org/10.1680/geot.2000.50.4.471

Foong, L.K., Rahman, N.A., Ramli, M.Z., 2016. A laboratory study of deformable double-porosity soil with distinct / (various) moisture content under vibration effect. Malaysian J. Civ. Eng. 28.

Fredlund, D.G., 2002. Use of soil–water characteristic curves in the implementation of unsaturated soil mechanics, in: Proceedings of the 3rd International Conference on Unsaturated Soils. Recife - PE, pp. 10–13.

Futai, M.M., Almeida, M.S.S., 2005. An experimental investigation of the mechanical behaviour of an unsaturated gneiss residual soil. Géotechnique 55, 201–213. https://doi.org/10.1680/geot.55.3.201.61520

Gens, A., Valleján, B., Sánchez, M., Imbert, C., Villar, M. V., van Geet, M., 2011. Hydromechanical behaviour of a heterogeneous compacted soil: Experimental

observations and modelling. Geotechnique 61, 367–386. https://doi.org/10.1680/geot.SIP11.P.015

Guimarães, R.C., 2002. Analysis of the properties and behaviour of a laterite soil profile applied to the study of the performance of excavated piles (in portuguese). Univ. Bras. University of Brasilia.

Hird, R., Bolton, M.D., 2017. Clarification of capillary rise in dry sand. Eng. Geol. 230, 77–83. https://doi.org/10.1016/j.enggeo.2017.09.023

Hoffmann, C., Alonso, E.E., Romero, E., 2007. Hydro-mechanical behaviour of bentonite pellet mixtures. Phys. Chem. Earth, Parts A/B/C 32, 832–849. https://doi.org/10.1016/j.pce.2006.04.037

Lloret, A., Villar, M. V., Sànchez, M., Gens, A., Pintado, X., Alonso, E.E., 2003. Mechanical behaviour of heavily compacted bentonite under high suction changes. Geotechnique 53, 27–40. https://doi.org/10.1680/geot.2003.53.1.27

Lopes, B. de C.F.L., 2016. Microstructural based approach to the modelling of clays and transitional soils behaviour. University of Brasília.

Lopes, B., Neto, M., Tarantino, A., 2014. An approach to detect microand macro-porosity from MIP data, in: Unsaturated Soils: Research & Applications. CRC Press, pp. 685–689. https://doi.org/10.1201/b17034-96

Lu, N., 2016. Generalized Soil Water Retention Equation for Adsorption and Capillarity. J. Geotech. Geoenvironmental Eng. 142, 04016051. https://doi.org/10.1061/(ASCE)GT.1943-5606.0001524

Lu, N., Dong, Y., 2017. Correlation between Soil-Shrinkage Curve and Water-Retention Characteristics. J. Geotech. Geoenvironmental Eng. 143, 04017054.

https://doi.org/10.1061/(ASCE)GT.1943-5606.0001741

Maccarini, M., 1987. Laboratory studies of a weakly bonded artificial soil. University of London.

Miguel, M.G., Bonder, B.H., 2012. Soil–Water Characteristic Curves Obtained for a Colluvial and Lateritic Soil Profile Considering the Macro and Micro Porosity. Geotech. Geol. Eng. 30, 1405–1420. https://doi.org/10.1007/s10706-012-9545-y

Mitchell, J.K., Soga, K., 2005. Fundamentals of Soil Behavior, 3rd Editio. ed. John Wiley and Sons.

Morgenstern, N.R., Tchalenko, J.S., 1967. Microscopic Structures in Kaolin Subjected to Direct Shear. Géotechnique 17, 309–328. https://doi.org/10.1680/geot.1967.17.4.309

Ng, C.W.W., Mu, Q.Y., Zhou, C., 2017. Effects of soil structure on the shear behaviour of an unsaturated loess at different suctions and temperatures. Can. Geotech. J. 54, 270–279. https://doi.org/10.1139/cgj-2016-0272

Otálvaro, I.F., Neto, M.P.C., Caicedo, B., 2015. Compressibility and microstructure of compacted laterites. Transp. Geotech. 5, 20–34. https://doi.org/10.1016/j.trgeo.2015.09.005

Otálvaro, I.F., Neto, M.P.C., Delage, P., Caicedo, B., 2016. Relationship between soil structure and water retention properties in a residual compacted soil. Eng. Geol. 205, 73–80. https://doi.org/10.1016/j.enggeo.2016.02.016

Pedrotti, M., 2016. An experimental investigation on the micromechanisms of non-active clays in saturated and partially saturated states. University of Strathclyde.

Pedrotti, M., Tarantino, A., 2014. Microstructural interpretation of compression behaviour of compacted kaolin clay, in: Unsaturated Soils: Research & Applications. CRC Press, pp.

739–745. https://doi.org/10.1201/b17034-104

Peng, X., Horn, R., 2005. Modeling Soil Shrinkage Curve across a Wide Range of Soil Types. Soil Sci. Soc. Am. J. 69, 584–592. https://doi.org/10.2136/sssaj2004.0146

Penumadu, D., Dean, J., 2000. Compressibility effect in evaluating the pore-size distribution of kaolin clay using mercury intrusion porosimetry. Can. Geotech. J. 37, 393–405. https://doi.org/10.1139/cgj-37-2-393

Queiroz, A.C.G., 2015. Study of the microstructural behaviour of compacted tropical soils (in portuguese). University of Brasília.

Rahardjo, H., Heng, O.B., Choon, L.E., 2004. Shear strength of a compacted residual soil from consolidated drained and constant water content triaxial tests. Can. Geotech. J. 41, 421–436. https://doi.org/10.1139/T03-093

Romero, E., 2013. A microstructural insight into compacted clayey soils and their hydraulic properties. Eng. Geol. 165, 3–19. https://doi.org/10.1016/j.enggeo.2013.05.024

Romero, E., 1999. Characterisation and Thermo Hydro-mechanical Behaviour of Unsaturated Boom Clay: An Experimental Study. Universitat Politècnica de Catalunya.

Romero, E., Simms, P.H., 2008. Microstructure investigation in unsaturated soils: A review with special attention to contribution of mercury intrusion porosimetry and environmental scanning electron microscopy. Geotech. Geol. Eng. 26, 705–727. https://doi.org/10.1007/s10706-008-9204-5

Sa'ari, R., Rahman, N.A., Abdul Latif, H.N., Yusof, Z.M., Ngien, S.K., Kamaruddin, S.A., Mustaffar, S.A., Hezmi, M.A., 2015. Application Of Digital Image Processing Technique In Monitoring LNAPL Migration In Double Porosity Soil Column. J. Teknol. 72, 23–29. https://doi.org/10.11113/jt.v72.4018

686 Sánchez, M., Gens, A., Villar, M.V., Olivella, S., 2016. Fully Coupled Thermo-Hydro-
687 Mechanical Double-Porosity Formulation for Unsaturated Soils. Int. J. Geomech. 16, 1–
688 17. https://doi.org/10.1061/(ASCE)GM.1943-5622.0000728

689 Serna, M.A.L., 2012. Applications of the material point method (MPM) on geotechnical
690 problems (in Portuguese). University of Brasília.

691 Silva, J.P. da, 2007. Preliminary studies for the implantation of infiltration trenches (in
692 Portuguese). University of Brasília.

693 Silva, M.T. de M.G., 2009. Methodology for determining parameters for unsaturated soils
694 using tests with known moisure (in portuguese). University of Brasilia.

695 Sivakumar, V., Sivakumar, R., Murray, E.J., Mackinnon, P., Boyd, J., 2010. Mechanical
696 behaviour of unsaturated kaolin (with isotropic and anisotropic stress history). part 1:
697 Wetting and compression behaviour. Geotechnique 60, 581–594.
698 https://doi.org/10.1680/geot.8.P.007

699 Sridharan, A., Prakash, K., 1998. Characteristic water contents of a fine-grained soil-water
700 system. Geotechnique 48, 337–346. https://doi.org/10.1680/geot.1998.48.3.337

701 Sridharan, A., Rao, S.M., Murthy, N.S., 1988. Liquid limit of kaolinitic soils. Geotechnique
702 38, 191–198. https://doi.org/10.1680/geot.1988.38.2.191

703 Tarantino, A., De Col, E., 2008. Compaction behaviour of clay. Geotechnique 58, 199–213.
704 https://doi.org/10.1680/geot.2008.58.3.199

705 Tarantino, A., Tombolato, S., 2005. Coupling of hydraulic and mechanical behaviour in
706 unsaturated compacted clay. Geotechnique 55, 307–317.
707 https://doi.org/10.1680/geot.2005.55.4.307

708 Thom, R., Sivakumar, R., Sivakumar, V., Murray, E.J., Mackinnon, P., 2007. Pore size

709 distribution of unsaturated compacted kaolin: the initial states and final states following
710 saturation. Géotechnique 57, 469–474. https://doi.org/10.1680/geot.2007.57.5.469

711 Tuller, M., Or, D., 2005. Water films and scaling of soil characteristic curves at low water
712 contents. Water Resour. Res. 41, 1–6. https://doi.org/10.1029/2005WR004142

713 Unger, P.W., Mccalla, T.M., 1980. Conservation Tillage Systems. Adv. Agron. 33, 1–58.

714 van Genuchten, M.T., 1980. A Closed-form Equation for Predicting the Hydraulic
715 Conductivity of Unsaturated Soils. Soil Sci. Soc. Am. J. 44, 892–898.
716 https://doi.org/10.2136/sssaj1980.03615995004400050002x

717 Venkatarama Reddy, B. V., Jagadish, K.S., 1993. The static compaction of soils.
718 Geotechnique 43, 337–341. https://doi.org/10.1680/geot.1993.43.2.337

719 Villibor, D.F., Nogami, J.S., 2009. Economic Pavements - Technology for the use of fine
720 laterite soils (in portuguese).

721 Wang, J.-D., Li, P., Ma, Y., Vanapalli, S.K., 2019. Evolution of pore-size distribution of
722 intact loess and remolded loess due to consolidation. J. Soils Sediments 19, 1226–1238.
723 https://doi.org/10.1007/s11368-018-2136-7

724 Wang, J.D., Li, P., Ma, Y., Vanapalli, S.K., Wang, X.G., 2020. Change in pore-size
725 distribution of collapsible loess due to loading and inundating. Acta Geotech. 15, 1081–
726 1094. https://doi.org/10.1007/s11440-019-00815-9

727 Wheeler, S.J., Sivakumar, V., 1995. An elasto-plastic critical state framework for unsaturated
728 soil. Geotechnique 45, 35–53. https://doi.org/10.1680/geot.1995.45.1.35

729 Yu, C.Y., Chow, J.K., Wang, Y.H., 2016. Pore-size changes and responses of kaolinite with
730 different structures subject to consolidation and shearing. Eng. Geol. 202, 122–131.
731 https://doi.org/10.1016/j.enggeo.2016.01.007

732

Micro-structural and volumetric behaviour of bimodal artificial soils with aggregates

Vinícius de Oliveira Kühn[a]

[a] Universidade Federal do Oeste da Bahia, Centro das Ciências Exatas e Tecnologias, Barreiras, Bahia, 47808-021, Brazil, vinicius.kuhn@ufob.edu.br, 0000-0001-5648-4372, corresponding author

Bruna de Carvalho Faria Lima Lopes[b]

[b] University of Strathclyde, Civil and Environmental Engineering Department, Glasgow, G1 1XJ, Scotland, UK, bruna.lopes@strath.ac.uk, 0000-0001-7669-7236

Bernardo Caicedo[c]

[c] Universidad de Los Andes, Civil and Environmental Engineering Department, Bogotá, Bogotá, 111711, Colômbia, bcaicedo@uniandes.edu.co, 0000-0003-4344-0914

Manoel Porfírio Cordão Neto[d]

[d] Universidade de Brasília, Departamento de Engenharia Civil e Ambiental, Faculdade de Tecnologia, Brasília, DF, 70910-900, Brazil, porfirio@unb.br, 0000-0003-0618-4376

Abstract

~~Tropical residual b~~Bimodal soils with aggregates present a complex micro-structural and volumetric ~~hydro-mechanical~~ behaviour~~, which is related to the presence of aggregates and elaborate structure~~. This occurs because ~~Behavioural models for these soils are difficult to develop since~~ they showcase several variables, ~~mainly~~ such as mineralogical, different grain sizes and structures. ~~and structural.~~ The objective of this paper is to develop a methodology for producing soils with aggregates and simple, non-mineralogical variability and controlled double porosity~~ structures representative of those of tropical residual soils, in which the bimodal pore structure is characterized by a large difference between the dominant micro and macro pores.~~ . In this sense, aggregates using Kaolin ~~clay~~ were created to obtain bimodal samples. The aggregates produced with this methodology were stable in water and the bimodal samples were analysed by means of Mercury Intrusion Porosimetry (MIP), Scanning Electron Microscopy (SEM), Soil Water Retention Curve (SWRC) and analysis of the shrinking process. Results show that the presence of aggregates in different proportions has a direct

impact on soil's: plasticity; classification; compaction curve; retention curve; as well as the pore size distribution (PSD), where ~~great difference in the sizes between dominant~~ micro and macro pores were observed. The shrinking and expansion analysis of the samples show that the presence of aggregates reduced both the expansive and shrinking potential. During the analysis of the shrinking process a fitting equation is presented to describe the trend of volumetric strain of the samples, from which it was possible to separate the soil shrinking process associated with the drying of the macro and microstructure and its relationship with the retention curve. Therefore, this study contributes to a better understanding of the role of aggregates on the microstructural and volumetric behaviour of ~~tropical residual~~bimodal soils.

Keywords

Bimodal soil; aggregates; kaolin~~ clay~~; soil structure; pore size distribution~~; residual soils.~~; volume change.

1. Introduction

Soil aggregates are secondary units which results from the binding of several soil particles (Unger and Mccalla, 1980). Soil aggregates play a major role in the formation of soil structure, which in turn influences the ~~hydro-mechanical~~soil's behaviour ~~of soils~~. The most well-known example of aggregates influence in the ~~hydro-mechanical~~ behaviour of soils comes from the field of geological repositories for nuclear waste disposal, where highly compacted bentonite blocks and mixtures of bentonite powder, pellets and sand are often used as the main engineered barrier systems protecting the groundwater and soil from contamination (Alonso et al., 2011; Gens et al., 2011; Hoffmann et al., 2007; Lloret et al., 2003; Sánchez et al., 2016).

However, aggregates are also observed in other contexts. Delage (2009) in discussion with Tarantino and De Col (2008) noticed that the distribution of bimodal pores in compacted Kaolin samples produced in their study was linked to the aggregates formed during the process of wetting and sieving carried out during the samples' preparation stage. Bagherieh et al. (2009) and Foong et al. (2016) made similar observations using similar procedures. In these cases the aggregates formed by the wetting and sieving procedures are easily destroyed. That is, they do not affect the geotechnical characteristics of the material, such as grain size distribution curve, compaction curve and Atterberg limits.

Additionally, aggregates can also be found in natural bimodal ~~residual~~ soils (Mitchell and Soga, 2005; Ng et al., 2017; Wang et al., 2019, 2020). Nevertheless, in tropical residual soils this is a remarkable characteristic. The weathering process of ~~tropical~~ residual soils, particularly in well-drained regions, promote the formation of soils aggregates with a bimodal pore structure characterized by a large difference between the dominant micro and macro pores (Cordão Neto et al., 2018; Futai and Almeida, 2005; Guimarães, 2002; Lopes, 2016; Miguel and Bonder, 2012; Otálvaro et al., 2016, 2015; Queiroz, 2015; Silva, 2007, 2009), ~~. In these cases, the aggregates have a high stability in water due to the presence of cementing agents.,~~ where the micro-porosity is formed by intra-aggregate spaces and macro-porosity is formed by inter-aggregate spaces (Alonso, 1998; Alonso et al., 1999; Mitchell and Soga, 2005; Romero, 2013; Romero and Simms, 2008). In these cases, the aggregates have a high stability in water due to the presence of cementing agents. ~~This double porosity feature has been observed in several studies, either when analysing the water retention or the pore size distribution (PSD) curves~~

~~Natural tropical residual soils have several complexities related with the high variability of geotechnical properties resulting from the process of chemical weathering, and the presence of different minerals and cementing agents such as iron and aluminium oxides and hydroxides . All these complexities make it difficult to understand the aggregates role on the soil structure hence hydro-mechanical behaviour of these soils.~~

Despite previous studies on bimodal soils with aggregates, it is not clear what are their effects on the soil's engineering behaviour. Inspired by pioneering work of Burland (1990), Bressani (1990), Maccarini (1987) and others, that turned to the creation of artificial soils to help in the understanding of fundamental soil behaviour, this study purposes the development of a methodology for producing soils with simple structures, ~~(~~non-mineralogical variability and controlled double porosity with aggregates.~~)~~ ~~representative of those of residual tropical soils, in which the bimodal pore structure is characterized by a large difference between the dominant micro and macro pores. In this sense, it is expected that this study could contribute to a better understanding of the role of aggregates on the microstructural behaviour of tropical residual soils.~~

Thus, the characteristics of the artificial bimodal soils produced are discussed in microstructural terms by means of Mercury Intrusion Porosimetry (MIP), Scanning Electron Microscopy (SEM), Soil Water Retention curve (SWRC) and shrinking process. ~~A parallel is also drawn among the differences between (1) the artificial soil with aggregates created and its counterpart original soil; and (2) the artificial soil with aggregates created and the inspirational natural tropical residual soils characterised by a large difference between the dominant micro and macro pores (Cordão Neto et al., 2018; Lopes, 2016; Miguel and Bonder, 2012).~~

2. Methodology for producing soils with controlled double porosity

Kaolin ~~Clay~~ was the material selected here to be used in the production of a control double porosity soil, as this material is basically composed of Kaolinite mineral; therefore it is a pure and classic material with non-mineralogical variability also adopted in several studies based on artificial ~~clayey~~ soils (Alazaiza et al., 2016; Bagherieh et al., 2009; Foong et al., 2016; Lopes, 2016; Morgenstern and Tchalenko, 1967; Pedrotti and Tarantino, 2014; Sa'ari et al., 2015; Serna, 2012; Tarantino and De Col, 2008; Tarantino and Tombolato, 2005; Wheeler and Sivakumar, 1995; Yu et al., 2016).

The material used in the research was Kaolin 605-635, produced in Brazil. Some of the characteristics of the material include: liquid limit, w_L, of 54.6%, plastic limit, w_p, of 38.5%, resulting in a plastic index, PI, of 16.1%; specific gravity, Gs, of 2.54; the proportion of clay-sized (particle size smaller than 2 μm) is 55% while the proportion of silt-sized (particle size between 2 μm and 75 μm) is 45%; this soil is classified as high plasticity silt (MH) according to the Unified Soil Classification System (USCS).

The methodology proposed for the development of a control double porosity material is presented in Figure 1 and consists of: (i) initial compaction of Kaolin ~~clay~~ at high stress - in order to generate a soil with stable aggregates (Figure 1a); (ii) remoulding new samples by mixing a pre-determined proportion of the sample created in Figure 1a, properly oven dried and crushed, with a proportion of the original supplied Kaolin ~~clay~~ (Figure 1b); (iii) new

compaction of samples produced in Figure 1b at a new moisture content (Figure 1c). This methodology is described in details in the following sections.

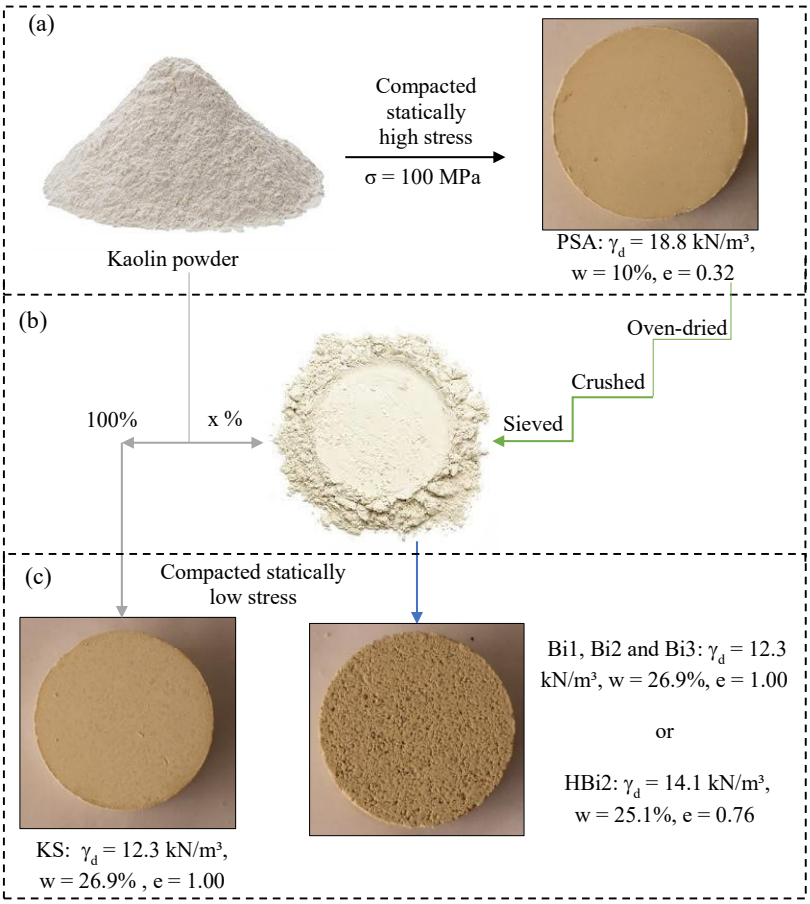

Figure 1 – Methodology for preparing bimodal samples: (a) high pressure compaction stage; (b) mixing step in different aggregate proportions; (c) low pressure compaction to obtain bimodal samples.

2.1 Preparation and characterization of artificial aggregates

As a starting point for obtaining artificial aggregates, compaction tests were performed using Standard Proctor and Mini Proctor (Villibor and Nogami, 2009) methodologies. The Kaolin ~~clay~~ powder was moistened and left to equilibrate for at least 24 hours before compaction. Figure 2a shows the compaction curves generated by these two methodologies; it can be observed a good agreement between the compaction curves obtained with the Standard Proctor's energy and the Mini Proctor test, which highlights the validity of the Mini Proctor test.

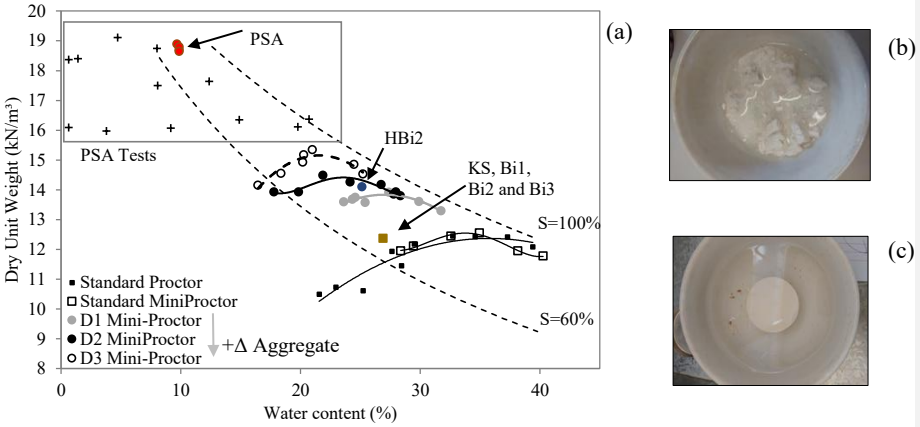

(b)

(c)

Figure 2 – (a) Compaction curves and stability tests to achieve stable microstructure; (b) unstable sample when submerged in water; (c) stable sample when submerged in water.

For the sake of producing artificial soils with controlled aggregate content ~~representative of natural residual soils~~, it is appropriate ~~to obtain~~that the aggregates ~~that~~ are stable when the material is immersed in water. This ensures that the aggregates remained in the samples at other preparation stages. Thus, after compaction, the stability of the samples was inspected by means of crumb tests (ASTM D6572, 2000), where samples were kept immersed in water for 12 hours,

149 double the recommended by the standard. This test provides a simple and quick method for
150 identifying dispersive clayey soil. Several crumb tests were performed on specimens coming
151 from static compaction at different stress levels (20, 40, 50, 100 MPa) and water contents (1%,
152 3%, 5%, 8%, 10%, 15%, 20%).
153
154 The strain rate of 1.2 mm/min was applied. ~~, and the target stress was maintained for 30 min to~~
155 ~~ensure homogeneity of the stress and redistribution of water within the sample.~~ This was similar
156 to that used by other authors in the literature (Rahardjo et al., 2004; Venkatarama Reddy and
157 Jagadish, 1993; Wheeler and Sivakumar, 1995). However, in the case under study, the sample
158 was kept under the final load for longer (30min) once the desired void ratio and stress level
159 were reached. This decision was a precaution made because the stress applied here (100 MPa)
160 is much greater than the conventional stress usually targeted. A time of 30 min was an extra
161 measure used to ensure the stress and water content distribution within the sample were
162 homogeneous or in the very least quasi-homogeneous, i.e., the excess pore-water pressure
163 generated by the application of the load dissipated before load was released. In the event that
164 the excess pore-water pressure does not dissipate before load was released an increase in
165 sample volume, hence void ratio, should be observed. No significant changes in the sample
166 volume after the compaction stage were observed (comparing the final void ratio obtained with
167 the targeted void ratio, standard deviation of 0.01 and coefficient of variation of 4.4%).
168
169 The points in Figure 2a represented by cross symbols show non-stable samples (Figure 2b)
170 while red circle points show the results of stable samples (Figure 2c) that were compacted
171 under 100 MPa at 10% of water content. This compaction produced samples that were stable
172 when immersed in water, here called Parent Sample of Aggregate (PSA), these samples had a

dry unit weight of 18.8 kN/m³, a degree of saturation of 80% and a void ratio of 0.32 (Figure 1a).

After obtaining a stable microstructure, the PSA samples were oven-dried at 105ºC (Figure 1b). In this temperature range there is no significant change in the kaolinite mineral (Caballero et al., 2019; Carneiro et al., 2003; Cheng et al., 2019). The oven-dried, crushed and sieved (sieve #10 – 2mm) material obtained from PSA samples are considered here the source of aggregates; and for this reason the word aggregates is here used as synonym for the material produced (PSA dried, crushed and sieved). Then, the material obtained was mixed with the originally supplied Kaolin powder ~~clay~~ in different proportions (Figure 1b). Three aggregate dosages were used. Dosage 1 had 100% of the mixed material passing through the 0.6 mm sieve, 80% through the 0.2 mm sieve and 60% through the 0.075 mm sieve. Dosage 2 reflected the grain size distribution of ~~Brasilia~~ a bimodal soil ~~(residual tropical soil)~~ provided by Otálvaro et al. (2015) without dispersant (100% passing through the 0.6 mm sieve, 57.8% through the 0.2 mm sieve and 37.5% through the 0.075 mm sieve). Finally, dosage 3 had 40% of the mixed material passing through the 0.2 mm sieve and 20% through the 0.075 mm sieve. That is, dosage 1 had the lowest percentage of aggregate (40%) distributed between fine and medium sand-sized diameters, dosage 3 had a higher aggregate content (80%) and dosage 2 intermediate aggregate content (62.5%). That is, aggregate content is the amount of dried, crushed and sieved PSA sample material used in each dosage.

The grain size distribution curves of kaolin samples, with and without dispersant, with different aggregate contents are shown in Figure 3a and b, respectively. These graphs show a prominent difference of the grain size distribution curve of the Kaolin ~~clay~~ with aggregate when

determined with and without dispersant. The grain size distribution curve of pure kaolin (dosage 0), without dispersant, shows no material of the size that conventionally characterises clay-sized particles; and stabilization of the curve in a diameter of 0.004 mm (Figure 3b). A higher percentage of clay-sized is observed in the grain size distribution curve of the same specimen (dosage 0) with dispersant (Figure 3a). This observation can be related to the effect of agglomeration and flocculation of clay-sized particles. This occurs due to electrostatic forces between the particles when immersed in an aqueous medium without a chemical dispersing agent, since this sample does not have aggregates.

~~As the aggregate content increases, there was a tendency for the curves without dispersant to move to the right of the pure kaolin curve (dosage 0). That is, dosage 3 in the graph without dispersant showed a larger sand diameter compared to dosage 2, followed by dosage 1. It is also apparent that the dispersant was able to eliminate the majority of aggregates. However, when comparing the grain size distribution, determined with dispersant, of pure Kaolin and Kaolin with aggregates, it is observed that some of the aggregates created in the Kaolin with aggregates samples were not completely wiped out. Perhaps the dispersing agent was not enough to eliminate all aggregates formed in the initial compaction stage.~~

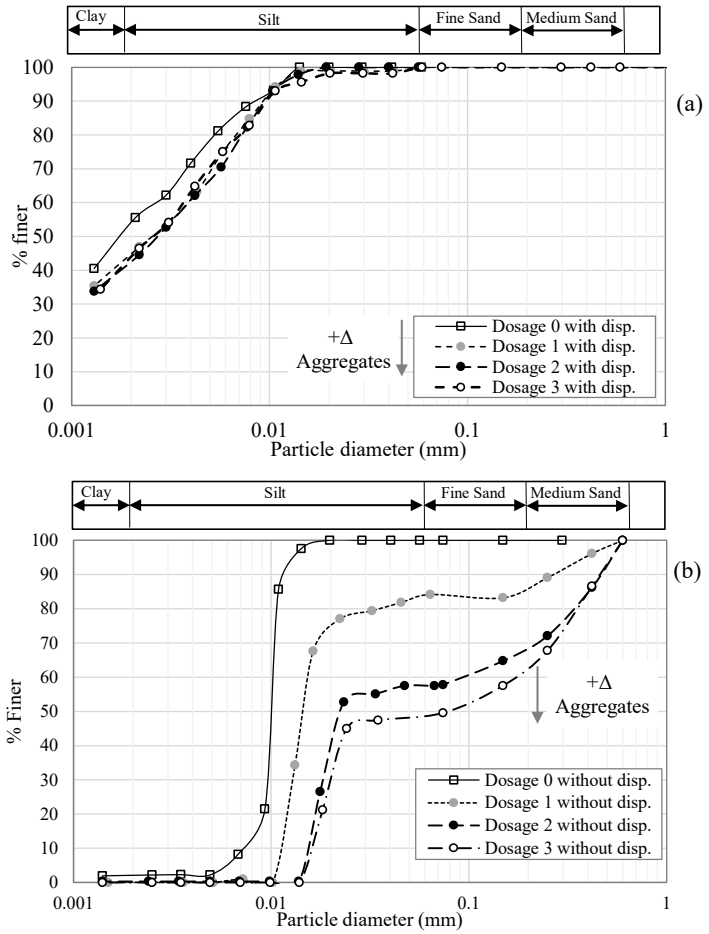

Figure 3 – Particle size distribution of Kaolin: (a) with dispersant; (b) without dispersant.

As the aggregate content increases, there was a tendency for the curves without dispersant to move to the right of the pure kaolin curve (dosage 0). That is, dosage 3 in the graph without dispersant showed a larger sand-sized diameter compared to dosage 2, followed by dosage 1. It is also apparent that the dispersant was able to eliminate the majority of aggregates. However, when comparing the grain size distribution, determined with dispersant, of pure Kaolin and Kaolin with aggregates, it is observed that some of the aggregates created in the Kaolin with

aggregates samples were not completely wiped out. Perhaps the dispersing agent was not enough to eliminate all aggregates formed in the initial compaction stage.

Atterberg limit tests were performed on all samples according to (ASTM D4318 (, 2017). The mixing prior to the liquid limit test was performed for 30 min. The plastic limit test was carried out after the liquid limit test. ~~previously discussed and~~ The results are shown in Figure 4. Since the presence of aggregate changed the soil consistency, it was observed that the increase in aggregates content generated a decrease in the liquid limit and plasticity index (Figure 4a). Consequently, there was a modification on the soil classification from MH to ML (USCS). Extrapolating the trend observed in these three aggregate levels (Figure 4b), ~~there is,~~ for a high aggregate content, there is convergence between w_L and w_p lines, which results in the complete loss of the plasticity index, similar to that observed in granular soils. Although the materials have the same mineralogy, the presence of aggregate reduced the specific surface of the particles, hence reducing their plasticity.

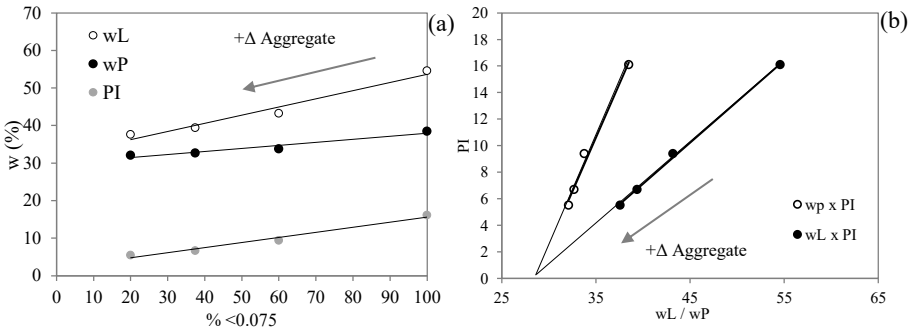

Figure 4 – Kaolin and Kaolin with aggregates: (a) Relationship between aggregate proportions and Atterberg limits; (b) Relationship between Atterberg limits and plasticity index.

Similar considerations were made by Sridharan et al. (1988) and Sridharan and Prakash (1998), who observed that the structure formed between particles affected the liquid limit. Along the same lines, Fearon and Coop (2000) observed an increase of the liquid limit and the plasticity index associated with the reconstitution of the sample and also with the energy and process of reconstitution. The authors observed significant differences between the Atterberg limits obtained depending on the method of reconstitution used: the standard procedure of hand mixing; passing the sample through a mixer; or passing it several times in a mincer. The observed tendency is an indecrease in the Atterberg limits with an increase in the energy use to reconstitute the samples. Similar to the tendency observed in this study, where an increase in aggregate content, which is the opposite to reconstitution, implicated in a decrease in the soil plasticity.

Regarding the compaction curves, it was noticed that the presence of kaolin aggregates generated a significant change in the compaction curve, with a decrease in the optimum water content and an increase in the dry unit weight (Figure 2a). Additionally, the shape of the compaction curve has narrowed with the increase of aggregate content.

2.2 Compaction of bimodal samples

These mixtures previously described (Figure 3) were used to obtain the compacted bimodal samples by means of static compaction at low stress. Two samples were produced from Dosage 2: (a) A sample compacted at a low energy to approach the dry branch of the compaction curve without aggregates (Figure 2a). The water content of this sample was w = 26.9% and the dry unit weight γ_d = 12.3 kN/m^3. This sample is herein referred to as Bimodal sample (Bi2); (b) A sample with aggregates produced with water content of 25.1% ~~subjected to the Standard~~

~~Proctor energy resulting in~~and ~~a~~ dry unit weight of γ_d=14.1 kN/m^3 (Figure 2a). This sample is herein referred to as High energy Bimodal sample (HBi2).

Two samples, compacted under the same water content and dry unit weight of Bi2, were produced from Dosage 1 and 3, herein named Bi1 and Bi3 respectively (Figure 2a). Another sample also compacted under the same water content and dry unit weight of Bi2, but now produced out of only Kaolin ~~clay~~, i.e., without the presence of aggregates, is denoted here as Kaolin Sample (KS). Thus, four samples produced from different dosage mixtures were created, compacted under the same water content and dry unit weight. In ascending order of aggregate content, they are: KS, Bi1, Bi2 and Bi3. Table 1 summarizes the origin and compaction conditions of the samples produced.

Sample	Origin	w (%)	γ_d (kN/m^3)	e
PSA	Pure Kaolin ~~Clay~~	10.0	18.8	0.32
KS	Pure Kaolin ~~Clay~~	26.9	12.3	1.00
Bi1	PSA and Pure Kaolin ~~Clay~~ dosage 1	26.9	12.3	1.00
Bi2	PSA and Pure Kaolin ~~Clay~~ dosage 2	26.9	12.3	1.00
HBi2	PSA and Pure Kaolin ~~Clay~~ dosage 2	25.1	14.1	0.76
Bi3	PSA and Pure Kaolin ~~Clay~~ dosage 3	26.9	12.3	1.00

Table 1 - Summary of origin and sample´s compaction conditions.

In order to prepare the samples for compaction, this procedure was followed: The kaolin ~~clay~~ material (Pure Kaolin ~~Clay~~ – dosage 0; or a mixture of Pure Kaolin ~~Clay~~ with PSA dried, crushed and sieve – dosage 1-3) was moistened using distilled water. After that the moistened material was sieved (sieve #10 – 2mm). The sieved material was stored in plastic bags for at least 24 hours before compaction. Finally, the material was moulded and statically compacted

at strain rates of 1.2 mm/min until the defined dry unit weight was reached. Samples were extruded using a dummy cylinder head. The standard deviation of the moisture content obtained for Bi and PSA samples was 0.31 and 0.34 respectively, while the standard deviation for the dry unit weight for Bi and PSA samples was 0.16 and 0.18 respectively.

2.3 Procedures for assessing the micro-structural behaviour

Parent Sample of Aggregate (PSA), Bimodal Samples (Bi1, Bi2 and Bi3), High Energy Bimodal Sample (HBi2) and Kaolin Sample (KS) were characterized by their SWRC, shrinkage curve and PSD, complemented with SEM images.

The ~~porosity~~ PSD of the specimens was measured using the MIP and qualitatively assessed by means of SEM images. Before carrying out the tests, specimens of 1 cm^3 in volume were prepared following freeze-drying. This technique consisted in applying rapid freezing with immersion in liquid nitrogen and then placing the specimen in a lyophilizer applying a pressure of 5 Pa and temperature of -50 °C for 24 hours. This methodology is reported by Delage and Lefebvre (1984) and Mitchell and Soga (2005) as the least disturbing freeze-drying procedure.

The SWRC was measured for the entire suction range using two testing procedures. To determine the SWRC, axis translation tests for suctions up to 500 kPa and dewpoint psychrometer (WP4C) for suctions above 500 kPa were used. Although the axis translation technique imposes matric suctions, and WP4C measures total suctions, both measurements showed a good agreement which allows the determination of one SWRC in terms of matric suction, in the same way performed by Tarantino and De Col (2008).

311

312 Fredlund (2002) integrated the shrinkage curve obtained by physical indexes (e versus w) with
313 the SWRC (w versus s), and noted that the shape of the shrinkage curve in terms of suction is
314 similar to the shape of the unimodal SWRC. Similar fittings of the shrinking process were also
315 performed by Peng and Horn (2005) and Cornelis et al. (2006). To obtain the shrinkage curve
316 (relationship between void ratio and water content), a caliper, an analytical balance and an oven
317 were used. The water content obtained was converted into suction using Durner´s fitting (1994)
318 from a previously determined SWRC. This procedure is similar to that adopted by Otálvaro et
319 al. (2016). Both, in the tests carried out for determining the SWRC, and in the tests performed
320 for determining the shrinkage curves, after compaction, specimens were wetted until the
321 capillarity saturation was reached and then they were submitted to drying paths. The capillary
322 saturation was performed by placing a porous stone and filter paper at the base of the sample
323 then the assembly was placed in an airtight container. Water added to the container comes into
324 contact with the porous stone and the soil absorbs water by capillarity upwards. This procedure
325 is similar to that adopted by Hird and Bolton (2017).

326

327 ## 3. Results and discussions

328 ### 3.1 Pore Size Distribution and Scanning Electron Microscopy

329 The results of the MIP tests were adjusted using an equation proposed by Durner (1994) and
330 adapted by Lopes et al. (2014) for bimodal soils. Figure 5a presents the results of the MIP tests
331 obtained for KS, Bi1, Bi2 and Bi3 samples (all of these were compacted under the same
332 conditions of water content and dry unit weight, having different aggregate content). The PSD
333 shown in Figure 5b is obtained by deriving the cumulative intrusion curves, as suggested by
334 Romero (1999). Figure 5c and d shows a comparative of samples prepared with the same

aggregate content but under different compaction conditions (water content, dry unit weight and void ratio).

The bimodal PSD of Bi2 and Bi3 samples observed in Figure 5b is unquestionable. The difference between the sizes of the dominant micro (≈ 0.1µm) and macro pores (≈ 100µm) in this samples reached 3 orders of magnitude. ~~It can be seen that a~~As the aggregate content increased, there was an increase in the size of the macro pores. On the other hand, in the micro pores range a higher frequency of pore diameters is observed, meanwhile the higher is the aggregate content the smaller are the diameters of micro pores noticed. In other words, it can be observed an increase in the bimodality of the samples as aggregate content rises. However, from Bi2 to Bi3 sample, despite an increase in the aggregate content, little change was observed in the macro pores region. ~~Likewise, it is clear that the increase of compaction energy led to a reduction of the macro pores, from Bi2 to HBi2 sample~~

It is important to note that previous researches showed little or no change on the micro pore after compaction and oedometer tests (Cordão Neto et al., 2018; Otálvaro et al., 2016; Wang et al., 2020). The difference observed in this paper in the micro-pores range is due to the stress level applied to PSA samples (100 MPa), that is far above the conventionally applied values found in the literature. Additionally, samples with the same aggregate content but compacted under different conventional energy levels (Bi2 and HBi2) show the same micro pore size. The increase in compaction energy in this case leads to a decrease only at the macro-pore level (Figure 5d). as observed in the aforementioned researches.~~.~~

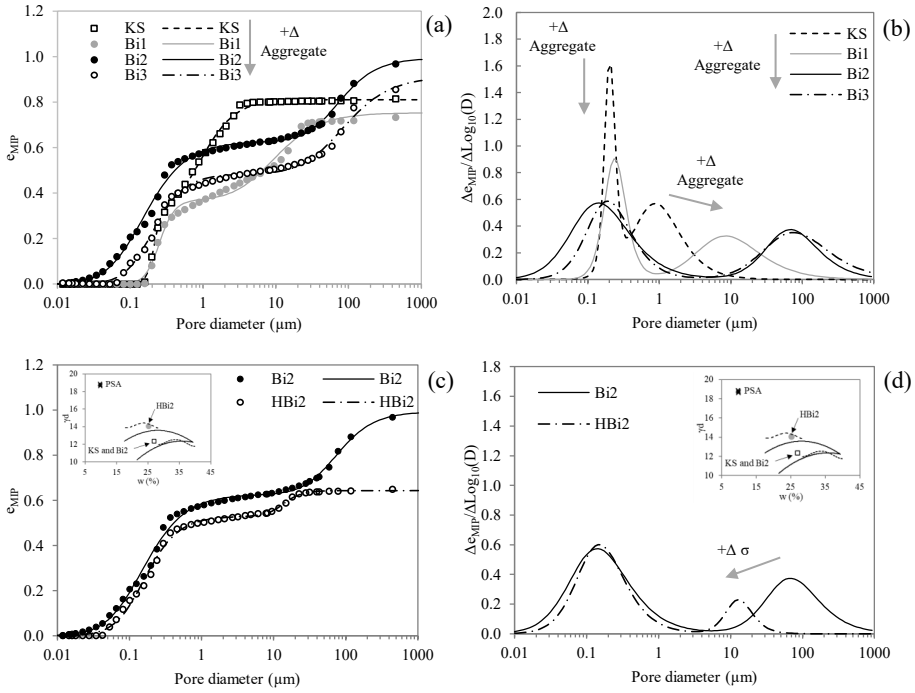

358

359

360 Figure 5 – MIP tests of KS, Bi1, Bi2 and Bi3: (a) Intrusion curve; (b) PSD; MIP tests of Bi2
361 and HBi2: (c) Intrusion curve; (d) PSD.

362

363 The KS sample, which is composed of only pure Kaolin ~~clay~~ and was compacted in the same
364 conditions ($w = 26.9\%$, $\gamma_d = 12.3$ kN/m³) as Bi2, presents slightly bimodal behaviour where the
365 difference between macro and micro pore sizes are not significant. Similar results have been
366 observed by other authors (Sivakumar et al., 2010; Tarantino and De Col, 2008; Thom et al.,
367 2007) in samples of compacted kaolin, and in samples of reconstituted kaolin at low vertical
368 stress levels (Lopes, 2016). At the same time, intermediate pore sizes (in the range of 2.0 μm)
369 observed in the KS sample are not present in the Bi2 sample.

370

371 The void ratios obtained by the MIP are smaller than the void ratios of the samples. The
372 difference is 0.06 for Bi2, 0.11 for HBi2, 0.26 for KS, 0.21 for Bi3 and 0.32 for Bi1 sample.

373 According to Romero and Simms (2008), this problem is usually observed in clayey soils due
374 to the difficulty of the mercury in filling the smaller pores of the soil, non-intruded porosity.
375 According to the authors, the differences between the void ratios can also be attributed to: (i)
376 isolated pores surrounded by solids which are not intruded; (ii) some pores which are accessible
377 only through smaller pores, i.e. they are not detected until smaller pores are penetrated,
378 restricted porosity; (iii) the minimum pressure of the apparatus limits the smallest pore size to
379 be detected, porosity not detected. Other researches have reported differences between the
380 voids ratios obtained by MIP in relation to the void ratios of the samples (Cordão Neto et al.,
381 2018; Lopes, 2016; Pedrotti, 2016). It is worth mentioning that some authors have also
382 observed the occurrence of compression on soft samples during the mercury intrusion phase
383 (Penumadu and Dean, 2000).

384

385 SEM imaging is a complementary method for analysing the soil's microstructure. Figure 6 and
386 Figure 7 show SEM images of the bimodal Bi2 and HBi2 samples at different scales. From
387 these figures, it is possible to recognise that Bi2 sample sustain a bimodal pore structures while
388 the increase in the compaction energy is responsible for the reduction of the macro pores
389 observed on the HBi2 sample (Figure 7). Considering the images of the HBi2 sample at the
390 larger scale, it is possible to notice that the aggregates formed over the high-energy compaction
391 have a predominantly face-to-face structure (Figure 7). Qualitatively, the images correspond to
392 the dominant pore sizes presented in Figure 5. These SEM images validate the proposed
393 methodology for preparing bimodal samples adopted in the research.

394

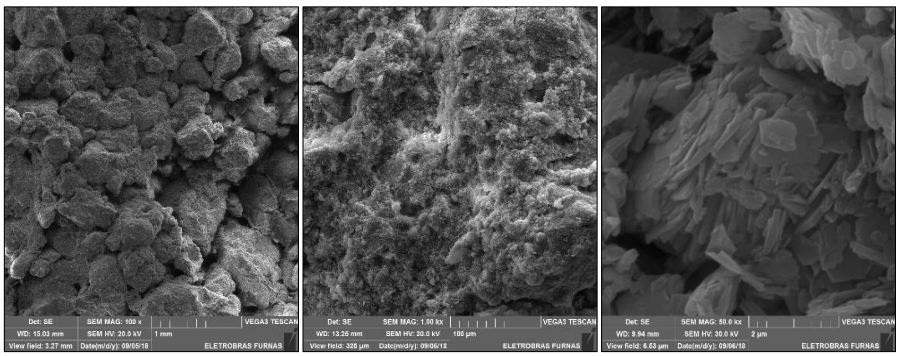

Figure 6 – SEM images of Bi2 sample.

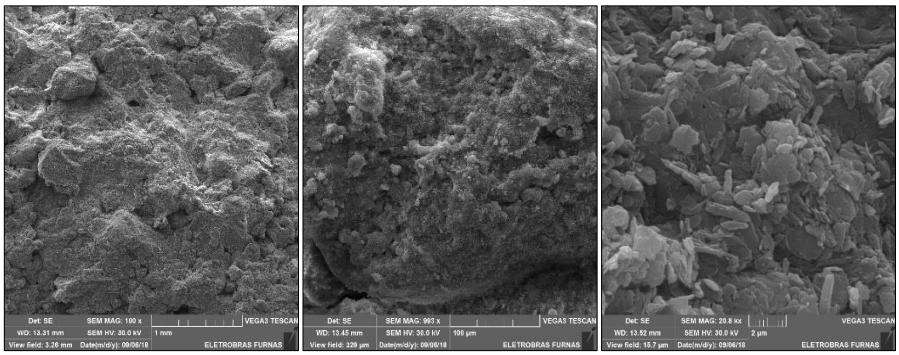

Figure 7 – SEM images of HBi2 sample.

~~In order to verify the bimodality of the samples produced in this research, a comparison of the PSDs obtained by MIP test was performed with results from other authors who studied tropical soils. To this end, the studies carried out by Miguel and Bonder (2012), Cordão Neto et al. (2018) and Lopes (2016) were used. Figure 8a shows the comparison of Bi2 sample with the Bimodal clay from Brasília in natural condition at 2 m depth (Cordão Neto et al., 2018; Lopes, 2016) and Figure 8b shows comparisons with samples from Campinas soil at two different depths, 1.5 m and 4.5 m (Miguel and Bonder, 2012).~~

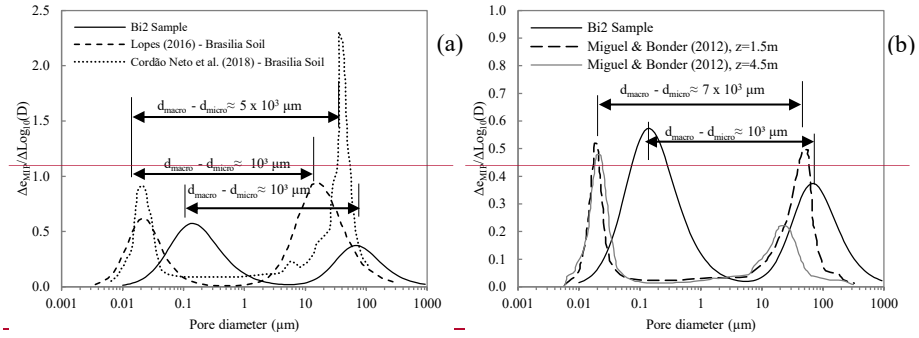

Figure 8 – Comparison between PSDs: (a) Kaolin Bi2 and Brasília soil in natural condition, Cordão Neto et al. (2018) and Lopes (2016); (b) Kaolin Bi2 and Campinas soil in natural condition, z = 1.5m and z = 4.5m, Miguel and Bonder (2012).

Based on Figure 8a, it can be seen that the distance between the dominant macro and micro pores of Bi2 sample is 3 orders of magnitudes, similar to the distance observed in the Brasília sample presented by Lopes (2016) and Cordão Neto et al. (2018). It is also observed that the dominant diameter of the macro and micro pores are not coincident. It is important to note that two different geo-materials are under comparison, therefore it is to be expected that the PSDs compared would be somehow different. Additionally, Brasília samples have in its mineralogy, in addition to kaolinite, cementing agents such as iron and aluminium oxides and hydroxides, which favour a more stable microstructure. Besides that, the porosimeters used in each case are also different, this could have an impact especially in the detection of smaller pore sizes.

Equivalent conclusions could be drawn when comparing Bi2 sample with Campinas soil (Miguel and Bonder, 2012) in Figure 8b. This soil is similar to Brasília soil hence Bi2, considering that they all show similar distances between the dominant macro and micro pores, and also micro pores in the same range of size.

3.2 Soil Water Retention Curves

The SWRC, expressed in terms of water ratio ($e_w = V_w / V_s$), was adjusted using Durner's (1994) equation, which is a generalization of the van Genutchen's equation (1980) for multimodal soils. For bimodal soils:

$$e_w = \frac{e_w^L}{\left[1+(a_L.s)^{n_L}\right]^{1-1/n_L}} + \frac{e_w^S}{\left[1+(a_S.s)^{n_s}\right]^{1-1/n_s}} \qquad \text{(Eq. 1)}$$

where: a and n are fitting parameters, s is suction, L and s subscriptions stand for large and small respectively.

Table 2 presents the fitting parameters used to adjust the SWRC. Figure 8a shows the SWRC of PSA, KS, Bi2 and HBi2, while Figure 8b shows the SWRC of KS, Bi1, Bi2 and Bi3 (in this last figure all samples were compacted under the same condition of water content and dry unit weight, having different aggregate contents).

~~The significant difference between the SWRC of the KS and Bi2 samples confirms that the proposed methodology is adequate for the creation of bimodal soils. Although both samples, KS and Bi2, were compacted under the same conditions of water content and void ratio, the presence of aggregates in Bi2 was determinant to produce a bimodal structure. In fact, for Bi2 sample (Figure 9a), water starts to drain out of the macro pores at a suction of 15 kPa and from the micro pores at 1500 kPa, which represents two orders of magnitude between the two porosities. On the other hand, in the KS sample it is not possible to clearly identify the level in which the draining within the macro pores ends and the draining amongst the micro pores begins (Figure 9a). In contrast, the higher density imposed on the compaction of the HBi2 sample reduced the size of the macro pores and the bimodal shape of the SWRC is less evident.~~

~~While the SWRC of the PSA sample presents unimodal characteristics due to the high energy applied during its constitution (100 MPa).~~

SWRC Fitting							Shrinkage curve Fitting						
	PSA	**KS**	**Bi1**	**Bi2**	**Bi3**	**HBi2**		**PSA**	**KS**	**Bi1**	**Bi2**	**Bi3**	**HBi2**
R^2	0.99	0.99	1.00	0.99	0.99	1.00	R^2	0.99	0.99	0.99	0.99	0.99	1.00
e_w^L	0.00	0.78	0.42	0.32	0.45	0.29	Δe^L	0.00	0.23	0.06	0.11	0.03	0.04
a_L	0.000	0.140	0.084	0.049	0.115	0.023	b_L	0.000	0.084	0.051	0.051	0.109	0.013
n_L	1.00	1.31	2.36	10.12	7.86	1.81	p_L	1.00	1.73	7.69	7.35	14.45	9.79
e_w^S	0.43	0.79	0.85	0.68	0.72	0.60	Δe^S	0.06	0.15	0.09	0.07	0.11	0.06
a_S	0.001	0.002	0.002	0.001	0.002	0.001	b_S	0.002	0.003	0.003	0.002	0.002	0.003
n_S	1.69	3.26	1.76	2.04	1.71	1.90	p_S	2.16	5.03	3.16	2.72	3.52	2.69
e_{wsat}	0.43	1.57	1.28	0.99	1.17	0.89	e_{res}	0.37	0.98	0.91	0.94	0.86	0.72
							e_{sat}	0.44	1.41	1.06	1.119	1.01	0.82

Table 2 – Fitting Parameter of SWRC and shrinkage curves.

The significant difference between the SWRC of the KS and Bi2 samples confirms that the proposed methodology is adequate for the creation of bimodal soils. Although both samples, KS and Bi2, were compacted under the same conditions of water content and void ratio, the presence of aggregates in Bi2 was determinant to produce a bimodal structure. In fact, for Bi2 sample (Figure 8a), water starts to drain out of the macro pores at a suction of 15 kPa and from the micro pores at 1500 kPa. On the other hand, in the KS sample it is not possible to clearly identify the level in which the draining within the macro pores ends and the draining amongst the micro pores begins (Figure 8a). In contrast, the higher density imposed on the compaction of the HBi2 sample reduced the size of the macro pores and the bimodal shape of the SWRC is less evident. While the SWRC of the PSA sample presents unimodal characteristics due to the high energy applied during its constitution (100 MPa).

~~The SWRCs show that the origin of the double porosity of the samples is considerably influenced by the presence of aggregates (Figure 9b). The trend is that the distance between macro and micro pores increases with the rise in the aggregate content, which is highlighted by the intermediate plateau of the SWRC of samples with aggregates. The suction value related to the air entry value of the macro pores show a decrease with the increase in aggregate content, and the micro pores a decrease in size caused by primary compaction process.~~

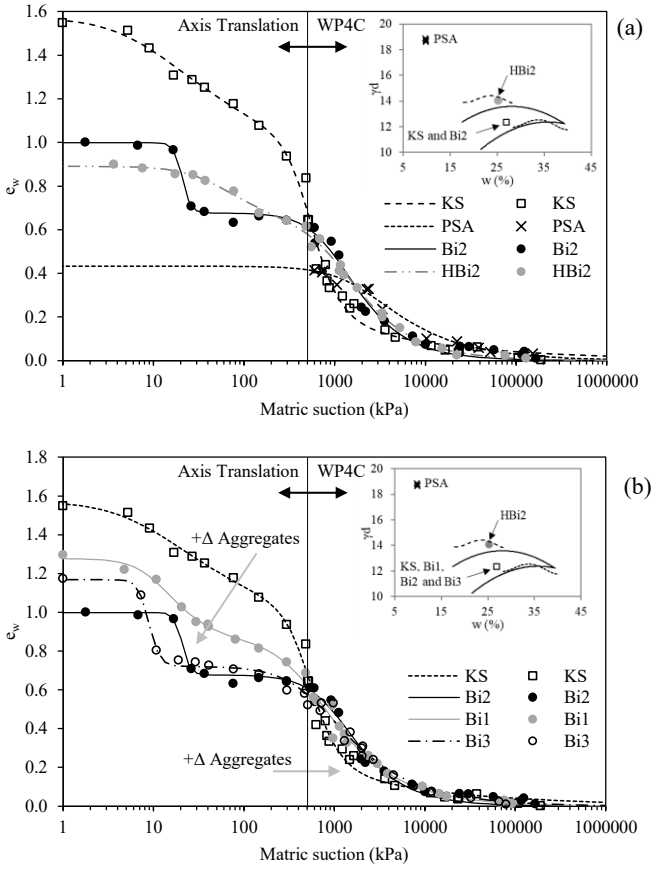

Figure 8 – Soil Water Retention Curve: (a) PSA, KS, Bi2 and HBi2; (b) KS, Bi1, Bi2 and Bi3.

The SWRCs show that the origin of the double porosity of the samples is considerably influenced by the presence of aggregates (Figure 8b). The trend is that the distance between macro and micro pores increases with the rise in the aggregate content, which is highlighted by the intermediate plateau of the SWRC of samples with aggregates. The suction value related to the air entry value of the macro pores show a decrease with the increase in aggregate content, and the micro pores a decrease in size caused by primary compaction process.

As the void ratio of the samples after the compaction process is the same (the only thing that differentiates the samples is the aggregate content), it is understood that the decrease in the diameters of micro pores with primary compaction and the formation of aggregates generated an increase in the macro pores of the samples~~,~~ ~~i~~In other words, a redistribution of the pores within the samples took place because the particles are now in an aggregated form. However, it is important to note that the presence of aggregates decreased the expansive potential of the samples, which also affects the redistribution of pores during the wetting and drying processes. The issues related to volumetric variation will be dealt with in the following section.

3.3 Volumetric behaviour and proposed shrinkage equation

The volumetric behaviour of the samples was evaluated during the wetting and drying process. Table 3 ~~-~~presents volumetric deformations, considering: the wetting phase, the drying phase and the total deformation.

Sample	$e_{initial}$	e_{sat}	$\varepsilon_{wetting}$ (%)	e_{final}	ε_{drying} (%)*	ε_{total} (%)**
PSA	0.31	0.49	-13.5	0.37	7.8	-4.7
KS	1.02	1.33	-15.3	0.99	14.4	1.3

Bi1	1.01	1.06	-2.9	0.90	7.9	5.2
Bi2	1.01	1.10	-4.5	0.94	7.6	3.5
Bi3	1.00	1.00	-0.3	0.85	7.6	7.4
HBi2	0.75	0.82	-3.7	0.72	5.5	2.0

*the initial void ratio considered is the e_{sat}, **the initial void ratio considered is $e_{initial}$.

Table 3 – Void ratios and volumetric deformations of samples subjected to wetting and drying.

The PSA and KS samples, when compared to the samples with aggregates (Bi1, Bi2, Bi3 and HBi2) present higher expansion once saturated while presenting higher skrinkage when drying (Table 3). This observation shows that (i) the presence of aggregates decreases the expansion and shrinkage, for wetting and drying respectively. And these reductions are also related with (ii) the reduction in the plasticity of Bi samples and eventually with (iii) the reduction on the specific surface which in turn is a product of the formation of aggregates. When comparing Bi2 and HBi2 samples (Table 3), the increase of energy during the secondary compaction process led to a reduction of the expansion potential of the HBi2 sample.

In terms of total volumetric deformation, it is observed that the PSA sample showed more expansion than shrinkage, which resulted in a negative total volumetric deformation, and non-recoverable deformations. The opposite is observed in the other samples, in which the final total deformation is positive, indicating more shrinkage than expansion, which is related to the structure formed during the compaction processes.

Thus, in samples with aggregates, during wetting, there is an expansion of aggregates generating a closure of macro pores with a slight variation in the total volume of the sample. The same occurs during the drying process, with shrinkage of aggregates and small variation

520 in total volume. This behaviour agrees with the analyses carried out by Romero (2013), which
521 demonstrated that the expansion of the microstructure by wetting can alter the macrostructure,
522 that is, there is an interaction between the different levels of structure (invasion or retraction of
523 macro pores due to expansion or shrinkage of micro pores). The observations here reported are
524 also in line with Alonso et al. (1999), who showed a trend of volumetric variation caused by
525 the expansion of the microstructure.

526

527 Regarding the shrinkage curves of the samples (Figure 9), a fitting equation based on Durner
528 (1994)'s proposal, with the intention of describing the shrinkage path of the soils, is suggested
529 for relating the void ratio of the sample to the suction during the drying path.

530

531 $$e = \frac{\Delta e^{L}}{\left[1+(b_L.s)^{p_L}\right]^{1-1p_L}} + \frac{\Delta e^{S}}{\left[1+(b_S.s)^{p_s}\right]^{1-1/p_s}} + e_{res} \qquad \text{(Eq. 2)}$$

532

533 where b and p are fitting parameters, e_{res} is the residual void ratio when reaching the non-
534 deformable state on drying, Δe^{L} and Δe^{S} represent the variation of voids ratio provided by the
535 drying of the macro and micro pores, respectively.

536

537 Table 2 shows the fitting parameters used to adjust the shrinkage curve. It is important to point
538 out that the parameter a_L (from SWRC) are close to the values of the fitting parameter b_L on
539 the corresponding shrinkage curve. The same observation could be drawn for the parameters
540 related to the drainage of the micro pores (a_s) and starting of the shrinkage, as a result of the
541 drying of the micro pores (b_s). The residual void ratio (e_{res}) is that obtained after the shrinking
542 limit of the soil, in which there is no more volumetric variation. Finally, the sum of the residual
543 void ratio (e_{res}) with the variation of the void ratio due to the shrinkage of the micro pores (Δe^{S})

and the variation of the void ratio due to the shrinkage of the macro pores (Δe^L) must be equal to the voids ratio of the saturated soil (e_{sat}).

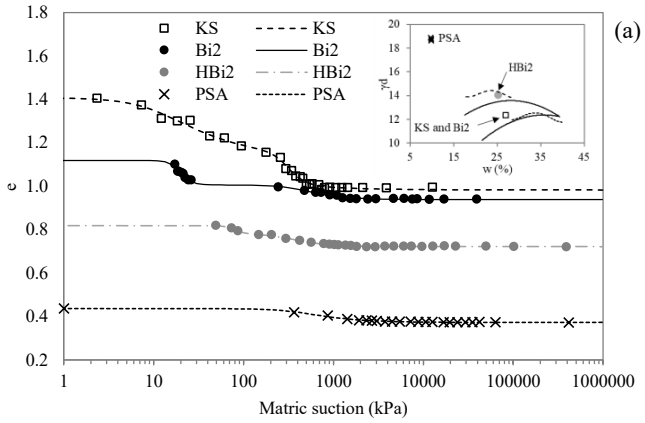

Figure 9 – Shrinkage curve of samples: (a) PSA, KS, Bi2 and HBi2; (b) KS, Bi1, Bi2 and Bi3.

~~Table 2 shows the fitting parameters used to adjust the shrinkage curve. It is important to point out that the parameter a_L (from SWRC) are close to the values of the fitting parameter b_L on the corresponding shrinkage curve. The same observation could be drawn for the parameters~~

Field Code Changed

~~related to the drainage of the micro pores (a_s) and starting of the shrinkage, as a result of the drying of the micro pores (b_s). The residual void ratio (e_{res}) is that obtained after the shrinking limit of the soil, in which there is no more volumetric variation. Finally, the sum of the residual void ratio (e_{res}) with the variation of the void ratio due to the shrinkage of the micro pores (Δe^S) and the variation of the void ratio due to the shrinkage of the macro pores (Δe^L) must be equal to the voids ratio of the saturated soil (e_{sat}).~~

The shrinkage curve of the PSA sample is fitted unimodally. As a result, equation 2 is reduced to two terms, as in the case of unimodal fittings one of the Δe becomes zero, and the fitting parameters b and p related to this term become obsolete. The remaining samples are fitted with the bimodal equation. In general, all fittings prove that the shrinkage fitting equation is quite effective in reproducing the shrinkage paths during drying (R^2 ranging from 0.99 to 1.00).

The shrinking behaviour occurs at different ranges of suction and is directly related to drainage of the macro and micro pores as represented by their SWRCs. Four shrinkage curves and their respective SWRC are presented: PSA (Figure 10a), Bi2 (Figure 10b), KS (Figure 10c) and Bi3 (Figure 10d). Indeed, regarding the bimodal samples the shrinking begins with the drainage of water from the macro pores and then continues with the drainage of the water from the micro pores. For example, for Bi2 sample (Figure 10b), it is observed that between suction of 30 and 200 kPa there is no drainage of water from the pores and, therefore, in this range there is no shrinking of the sample, as demonstrated by the experimental shrinkage data and corresponding fitting curve (Figure 10b). Similar observations can be drawn for other bimodal samples. On the other hand, the PSA sample characterised by unimodal SWRC shows shrinking beginning on the same suction range where the pore drainage begins (Figure 10a).

In all cases, shrinking within the micro pores occurs approximately halfway up the drainage section of the micro pores, until the samples reach a residual void ratio. This is due to the fact that shrinking is motivated by the increase of suction hence decrease of water meniscus in the soil. It appears that in the case under study, after half of the drainage of the micro pores, the water will no longer be in its capillary form, it is now immobile - only present in the form of meniscus, thus stopping soil shrinkage (Lu, 2016; Lu and Dong, 2017; Tuller and Or, 2005).

Based on the proposed fitting equation and the data presented in Table 2, it is possible to separate the variation in voids ratio associated with the drainage of micro and macro pores during the drying process, as well as to determine which suction values are thresholds responsible for the process of shrinkage of the samples.

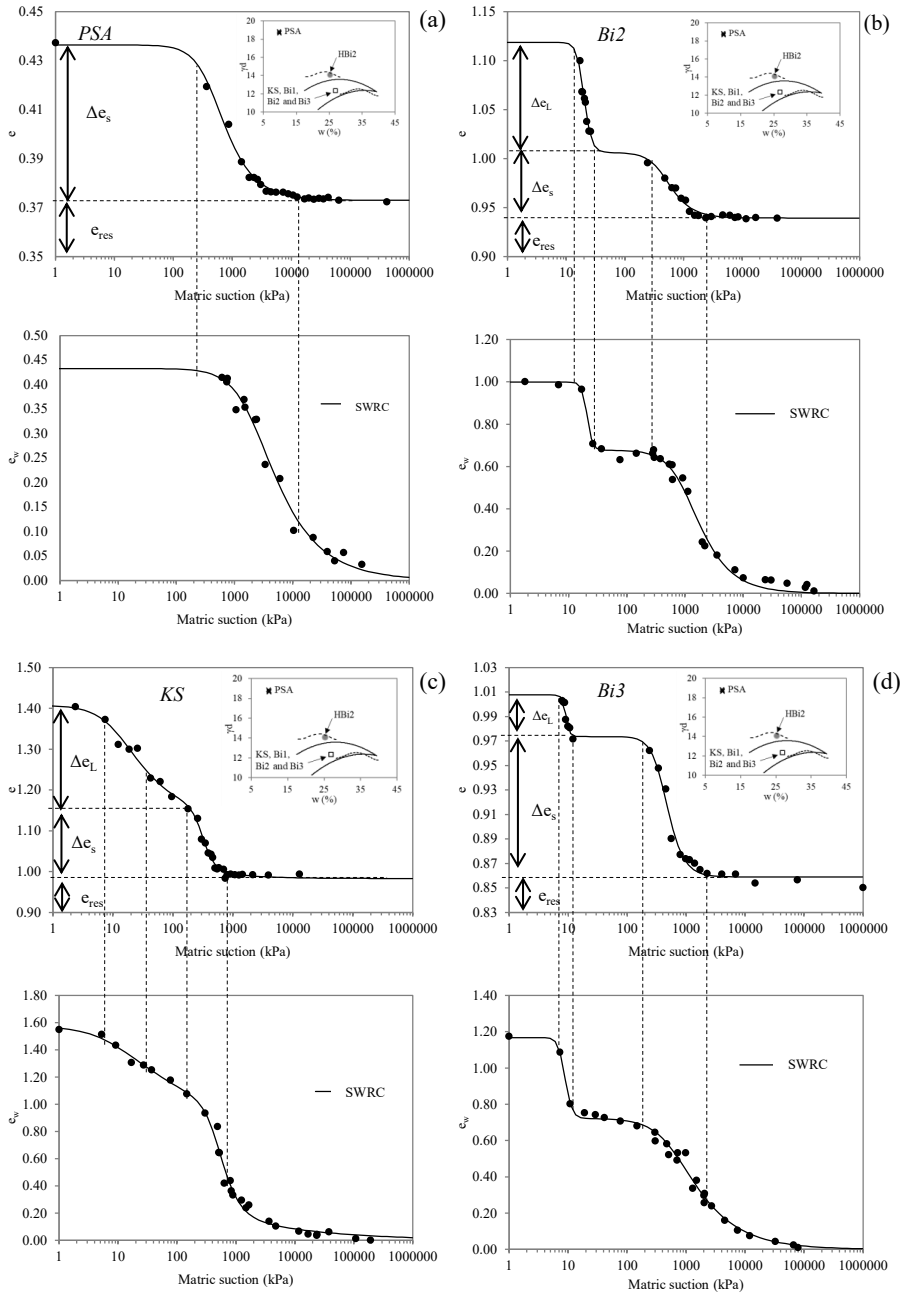

Figure 10 – (a) Shrinkage curves applied to proposed fitting equation, together with SWRC and interest points: (a) unimodal sample PSA; (b) bimodal sample Bi2; (c) KS; (d) Bi3.

~~In all cases, shrinking within the micro pores occurs approximately halfway up the drainage section of the micro pores, until the samples reach a residual void ratio. This is due to the fact that shrinking is motivated by the increase of suction hence decrease of water meniscus in the soil. It appears that in the case under study, after half of the drainage of the micro pores, the water will no longer be in its capillary form, it is now immobile – only present in the form of meniscus, thus stopping soil shrinkage (Lu, 2016; Lu and Dong, 2017; Tuller and Or, 2005).~~

~~Based on the proposed fitting equation and the data presented in Table 2, it is possible to separate the variation in voids ratio associated with the drainage of micro and macro pores during the drying process, as well as to determine which suction values are thresholds responsible for the process of shrinkage of the samples.~~

Field Code Changed

4. Conclusions

~~Tropical residual bimodal soils present a complex hydro-mechanical behaviour, which is related to the presence of aggregates and elaborate structure.~~ Previous ~~R~~researcher~~s~~s have recognised that the soil structure is one of the key soil elements that needs to be examined to allow for a fully comprehensive understanding of its ~~hydro-mechanical~~ behaviour. In the interest of contributing to a better understanding of the role of aggregates on the microstructural behaviour of ~~residual tropical~~bimodal soils ~~hence hydro-mechanical behaviour~~, this paper described a new methodology for producing soils with simple - non-mineralogical variability and controlled double porosity - structures ~~representative of those of residual tropical soils, in which the bimodal pore structure is characterized by a large difference between the dominant micro and macro pores.~~ .

The methodology proposed consisted in creating aggregate by compacting Kaolin ~~clay~~ at high stresses (100MPa). The product of this sample was then oven-dried, crushed, sieved and mixed in different proportions with additional Kaolin powder~~clay material~~ to create samples with different aggregate content. Thus, four samples were produced and compacted under the same conditions of water content, dry unit weight and void ratio, having different aggregate contents (0, 40, 62.5 and 80%). An additional sample, with 62.5% aggregate content was compacted targeting lower water content and void ratio and higher dry unit weight.

The aggregates within the samples created were stable in water, which is crucial to ensures that aggregates remained in the samples at other preparation stages. This also allows to control the aggregates content and the double porosity.~~for simulating natural tropical residual soils.~~ This stability ~~fact~~ was observed when comparing the grain size distribution of the different aggregate content samples without dispersant. Another important observation to be highlighted is that although the materials have the same mineralogy, the presence of aggregates reduced the specific surface of the particles, hence reducing their plasticity. This has also led to a decrease in expansivity with an increase in aggregate content. Additionally, the increase in aggregate content have also promoted change in the soil classification and compaction curve.

The samples created were assessed microstructurally by means of Soil Water Retention Curves (SWRC) and Pore Size Distribution (PSD), as well as qualitatively by Scanning Electron Microscopy (SEM) images. A relevant characteristic of the soils obtained with the proposed methodology is the bimodality. The difference between the sizes of the dominant micro and

macro pores reached ~~2 to~~ 3 orders of magnitude. ~~This characteristic had not been observed in previous kaolin researches and agreed with the differences between dominant sizes of micro and macro pores of natural tropical residual soils .~~ It was observed that the increase in the size of dominant macro pores is associated with the increase in aggregate content up to a point, since no significant change in the dominant macro pores were observed between samples with aggregate content of 62.5 and 80%. Furthermore, the increase in compaction density led to a reduction in the difference between the size of dominant micro and macro pores together with a slight change in the size of micro pores.

The microstructural behaviour of the bimodal soils was also studied through their shrinkage curves. These curves showed that the presence of aggregates decreased the expansion and shrinkage of the samples. Moreover, in terms of suction, the shrinkage curves show tendency of shrinking similarly to the drainage observed in the SWRC. Based on these results, a fitting equation based on the soils' volumetric strain behaviour was developed fitting successfully the experimental shrinkage data.

Additionally, it is important to highlight that the methodology proposed for preparing bimodal soils produces soils with aggregates and non-mineralogical complexity (i.e., macro pores and aggregates are both made out of Kaolin ~~Clay~~material), which emphasises difference between micro and macro structure. This characteristic could be extremely useful for differentiating the effect of the soil microstructure on ~~the~~ its macroscopic behaviour.

~~Finally, the comparison of the bimodal PSD of samples created in this research with samples of high weathering residual soils proved that it was possible to simulate successfully the~~

~~structure of these soils in laboratory using only one type of mineral, which favours further studies of hydro-mechanical analyses.~~

The next stages of the research involve ~~: (i)~~ assessing the hydro-mechanical characteristics of these artificial bimodal soils as well as the effects that the double porosity caused on them ~~and~~.~~:~~ ~~(ii) finally transferring the knowledge acquired with the microstructural, hydro-mechanical study of artificial bimodal soils to natural tropical residual bimodal soils.~~

Acknowledgements

The authors would like to thank the Geotechnics program of University of Brasília and Federal University of Western Bahia for the support provided to carry out this research as well as University of Los Andes and Eletrobrás Furnas. The authors would also like to acknowledge the Brazilian research council, the National Council for Scientific and Technological Development (CNPQ) for providing the funds for the acquisition of equipment used in this research.

References

Alazaiza, M.Y.D., Ngien, S.K., Bob, M.M., Kamaruddin, S.A., Faizal Ishak, W.M., 2016. Assessment of the behaviour of soil structure in double-porosity kaolin media using light transmission visualization (LTV) method. Int. J. Geotech. Eng. 11, 316–320. https://doi.org/10.1080/19386362.2016.1211370

Alonso, E.E., 1998. Modelling Expansive Soil Behaviour, in: Proceedings Of The Second International Conference On Unsaturated Soils. p. 7625.

Alonso, E.E., Romero, E., Hoffmann, C., 2011. Hydromechanical behaviour of compacted

granular expansive mixtures: experimental and constitutive study. Géotechnique 61, 329–344. https://doi.org/10.1680/geot.2011.61.4.329

Alonso, E.E., Vaunat, J., Gens, A., 1999. Modelling the mechanical behaviour of expansive clays. Eng. Geol. 54, 173–183. https://doi.org/10.1016/S0013-7952(99)00079-4

ASTM, 2017. D4318-17e1, Standard Test Methods for Liquid Limit, Plastic Limit, and Plasticity Index of Soils. West Conshohocken, PA.

ASTM, 2000. D 6572-12 Standard Test Methods for Determining Dispersive Characteristics of Clayey Soils by the Crumb Test. ASTM Int. 11, 3–6.

Bagherieh, A.R., Khalili, N., Habibagahi, G., Ghahramani, A., 2009. Drying response and effective stress in a double porosity aggregated soil. Eng. Geol. 105, 44–50. https://doi.org/10.1016/j.enggeo.2008.12.009

Bressani, L.A., 1990. Experimental properties of bonded soils. University of London.

Caballero, L.R., Paiva, M. das D.M., Fairbairn, E. de M.R., Toledo Filho, R.D., 2019. Thermal, Mechanical and Microstructural Analysis of Metakaolin Based Geopolymers. Mater. Res. 22, 1–8. https://doi.org/10.1590/1980-5373-mr-2018-0716

Carneiro, B.S., Angélica, R.S., Scheller, T., Castro, E.A.S. de, Neves, R.F., 2003. Mineralogical and geochemical characterization of the hard kaolin from the Capim region, Pará, northern Brazil (in portuguese). Cerâmica 49, 237–244. https://doi.org/10.1590/s0366-69132003000400008

Cheng, Xing, Bu, Zhang, Piao, Huang, Xie, Wang, 2019. Dehydroxylation and Structural Distortion of Kaolinite as a High-Temperature Sorbent in the Furnace. Minerals 9, 587. https://doi.org/10.3390/min9100587

Cordão Neto, M.P., Hernández, O., Lorenzo Reinaldo, R., Borges, C., Caicedo, B., 2018.

715 Study of the relationship between hydro-mechanical soil behavior and microstructure of
716 a structured soil. Earth Sci. Res. J. 22, 91–101.
717 https://doi.org/10.15446/esrj.v22n2.65640

718 Cornelis, W.M., Corluy, J., Medina, H., Díaz, J., Hartmann, R., Van Meirvenne, M., Ruiz,
719 M.E., 2006. Measuring and modelling the soil shrinkage characteristic curve. Geoderma
720 137, 179–191. https://doi.org/10.1016/j.geoderma.2006.08.022

721 Delage, P., 2009. DISCUSSION: Compaction behaviour of clay. A. TARANTINO and E.
722 DE COL (2008). Géotechnique 58 , No, 3, 199–213. Géotechnique 59, 75–77.
723 https://doi.org/10.1680/geot.2008.59.1.75

724 Delage, P., Lefebvre, G., 1984. Study of the structure of a sensitive Champlain clay and of its
725 evolution during consolidation. Can. Geotech. J. 21, 21–35. https://doi.org/10.1139/t84-
726 003

727 Durner, W., 1994. Hydraulic conductivity estimation for soils with heterogeneous pore
728 structure. Water Resour. Res. 30, 211–223. https://doi.org/10.1029/93WR02676

729 Fearon, R.E., Coop, M.R., 2000. Reconstitution: What makes an appropriate reference
730 material? Geotechnique 50, 471–477. https://doi.org/10.1680/geot.2000.50.4.471

731 Foong, L.K., Rahman, N.A., Ramli, M.Z., 2016. A laboratory study of deformable double-
732 porosity soil with distinct / (various) moisture content under vibration effect. Malaysian
733 J. Civ. Eng. 28.

734 Fredlund, D.G., 2002. Use of soil–water characteristic curves in the implementation of
735 unsaturated soil mechanics, in: Proceedings of the 3rd International Conference on
736 Unsaturated Soils. Recife - PE, pp. 10–13.

737 Futai, M.M., Almeida, M.S.S., 2005. An experimental investigation of the mechanical

738 behaviour of an unsaturated gneiss residual soil. Géotechnique 55, 201–213.
739 https://doi.org/10.1680/geot.55.3.201.61520

740 Gens, A., Valleján, B., Sánchez, M., Imbert, C., Villar, M. V., van Geet, M., 2011.
741 Hydromechanical behaviour of a heterogeneous compacted soil: Experimental
742 observations and modelling. Geotechnique 61, 367–386.
743 https://doi.org/10.1680/geot.SIP11.P.015

744 Guimarães, R.C., 2002. Analysis of the properties and behaviour of a laterite soil profile
745 applied to the study of the performance of excavated piles (in portuguese). Univ. Bras.
746 University of Brasilia.

747 Hird, R., Bolton, M.D., 2017. Clarification of capillary rise in dry sand. Eng. Geol. 230, 77–
748 83. https://doi.org/10.1016/j.enggeo.2017.09.023

749 Hoffmann, C., Alonso, E.E., Romero, E., 2007. Hydro-mechanical behaviour of bentonite
750 pellet mixtures. Phys. Chem. Earth, Parts A/B/C 32, 832–849.
751 https://doi.org/10.1016/j.pce.2006.04.037

752 Lloret, A., Villar, M. V., Sànchez, M., Gens, A., Pintado, X., Alonso, E.E., 2003. Mechanical
753 behaviour of heavily compacted bentonite under high suction changes. Geotechnique 53,
754 27–40. https://doi.org/10.1680/geot.2003.53.1.27

755 Lopes, B. de C.F.L., 2016. Microstructural based approach to the modelling of clays and
756 transitional soils behaviour. University of Brasília.

757 Lopes, B., Neto, M., Tarantino, A., 2014. An approach to detect microand macro-porosity
758 from MIP data, in: Unsaturated Soils: Research & Applications. CRC Press, pp. 685–
759 689. https://doi.org/10.1201/b17034-96

760 Lu, N., 2016. Generalized Soil Water Retention Equation for Adsorption and Capillarity. J.

761 Geotech. Geoenvironmental Eng. 142, 04016051.
762 https://doi.org/10.1061/(ASCE)GT.1943-5606.0001524

763 Lu, N., Dong, Y., 2017. Correlation between Soil-Shrinkage Curve and Water-Retention
764 Characteristics. J. Geotech. Geoenvironmental Eng. 143, 04017054.
765 https://doi.org/10.1061/(ASCE)GT.1943-5606.0001741

766 Maccarini, M., 1987. Laboratory studies of a weakly bonded artificial soil. University of
767 London.

768 Miguel, M.G., Bonder, B.H., 2012. Soil–Water Characteristic Curves Obtained for a
769 Colluvial and Lateritic Soil Profile Considering the Macro and Micro Porosity. Geotech.
770 Geol. Eng. 30, 1405–1420. https://doi.org/10.1007/s10706-012-9545-y

771 Mitchell, J.K., Soga, K., 2005. Fundamentals of Soil Behavior, 3rd Editio. ed. John Wiley
772 and Sons.

773 Morgenstern, N.R., Tchalenko, J.S., 1967. Microscopic Structures in Kaolin Subjected to
774 Direct Shear. Géotechnique 17, 309–328. https://doi.org/10.1680/geot.1967.17.4.309

775 Ng, C.W.W., Mu, Q.Y., Zhou, C., 2017. Effects of soil structure on the shear behaviour of an
776 unsaturated loess at different suctions and temperatures. Can. Geotech. J. 54, 270–279.
777 https://doi.org/10.1139/cgj-2016-0272

778 Otálvaro, I.F., Neto, M.P.C., Caicedo, B., 2015. Compressibility and microstructure of
779 compacted laterites. Transp. Geotech. 5, 20–34.
780 https://doi.org/10.1016/j.trgeo.2015.09.005

781 Otálvaro, I.F., Neto, M.P.C., Delage, P., Caicedo, B., 2016. Relationship between soil
782 structure and water retention properties in a residual compacted soil. Eng. Geol. 205,
783 73–80. https://doi.org/10.1016/j.enggeo.2016.02.016

784 Pedrotti, M., 2016. An experimental investigation on the micromechanisms of non-active
785 clays in saturated and partially saturated states. University of Strathclyde.
786 Pedrotti, M., Tarantino, A., 2014. Microstructural interpretation of compression behaviour of
787 compacted kaolin clay, in: Unsaturated Soils: Research & Applications. CRC Press, pp.
788 739–745. https://doi.org/10.1201/b17034-104
789 Peng, X., Horn, R., 2005. Modeling Soil Shrinkage Curve across a Wide Range of Soil
790 Types. Soil Sci. Soc. Am. J. 69, 584–592. https://doi.org/10.2136/sssaj2004.0146
791 Penumadu, D., Dean, J., 2000. Compressibility effect in evaluating the pore-size distribution
792 of kaolin clay using mercury intrusion porosimetry. Can. Geotech. J. 37, 393–405.
793 https://doi.org/10.1139/cgj-37-2-393
794 Queiroz, A.C.G., 2015. Study of the microstructural behaviour of compacted tropical soils (in
795 portuguese). University of Brasília.
796 Rahardjo, H., Heng, O.B., Choon, L.E., 2004. Shear strength of a compacted residual soil
797 from consolidated drained and constant water content triaxial tests. Can. Geotech. J. 41,
798 421–436. https://doi.org/10.1139/T03-093
799 Romero, E., 2013. A microstructural insight into compacted clayey soils and their hydraulic
800 properties. Eng. Geol. 165, 3–19. https://doi.org/10.1016/j.enggeo.2013.05.024
801 Romero, E., 1999. Characterisation and Thermo Hydro-mechanical Behaviour of Unsaturated
802 Boom Clay: An Experimental Study. Universitat Politècnica de Catalunya.
803 Romero, E., Simms, P.H., 2008. Microstructure investigation in unsaturated soils: A review
804 with special attention to contribution of mercury intrusion porosimetry and
805 environmental scanning electron microscopy. Geotech. Geol. Eng. 26, 705–727.
806 https://doi.org/10.1007/s10706-008-9204-5

807 Sa'ari, R., Rahman, N.A., Abdul Latif, H.N., Yusof, Z.M., Ngien, S.K., Kamaruddin, S.A.,
808 Mustaffar, S.A., Hezmi, M.A., 2015. Application Of Digital Image Processing
809 Technique In Monitoring LNAPL Migration In Double Porosity Soil Column. J. Teknol.
810 72, 23–29. https://doi.org/10.11113/jt.v72.4018

811 Sánchez, M., Gens, A., Villar, M.V., Olivella, S., 2016. Fully Coupled Thermo-Hydro-
812 Mechanical Double-Porosity Formulation for Unsaturated Soils. Int. J. Geomech. 16, 1–
813 17. https://doi.org/10.1061/(ASCE)GM.1943-5622.0000728

814 Serna, M.A.L., 2012. Applications of the material point method (MPM) on geotechnical
815 problems (in Portuguese). University of Brasília.

816 Silva, J.P. da, 2007. Preliminary studies for the implantation of infiltration trenches (in
817 Portuguese). University of Brasília.

818 Silva, M.T. de M.G., 2009. Methodology for determining parameters for unsaturated soils
819 using tests with known moisure (in portuguese). University of Brasilia.

820 Sivakumar, V., Sivakumar, R., Murray, E.J., Mackinnon, P., Boyd, J., 2010. Mechanical
821 behaviour of unsaturated kaolin (with isotropic and anisotropic stress history). part 1:
822 Wetting and compression behaviour. Geotechnique 60, 581–594.
823 https://doi.org/10.1680/geot.8.P.007

824 Sridharan, A., Prakash, K., 1998. Characteristic water contents of a fine-grained soil-water
825 system. Geotechnique 48, 337–346. https://doi.org/10.1680/geot.1998.48.3.337

826 Sridharan, A., Rao, S.M., Murthy, N.S., 1988. Liquid limit of kaolinitic soils. Geotechnique
827 38, 191–198. https://doi.org/10.1680/geot.1988.38.2.191

828 Tarantino, A., De Col, E., 2008. Compaction behaviour of clay. Geotechnique 58, 199–213.
829 https://doi.org/10.1680/geot.2008.58.3.199

Tarantino, A., Tombolato, S., 2005. Coupling of hydraulic and mechanical behaviour in unsaturated compacted clay. Geotechnique 55, 307–317. https://doi.org/10.1680/geot.2005.55.4.307

Thom, R., Sivakumar, R., Sivakumar, V., Murray, E.J., Mackinnon, P., 2007. Pore size distribution of unsaturated compacted kaolin: the initial states and final states following saturation. Géotechnique 57, 469–474. https://doi.org/10.1680/geot.2007.57.5.469

Tuller, M., Or, D., 2005. Water films and scaling of soil characteristic curves at low water contents. Water Resour. Res. 41, 1–6. https://doi.org/10.1029/2005WR004142

Unger, P.W., Mccalla, T.M., 1980. Conservation Tillage Systems. Adv. Agron. 33, 1–58.

van Genuchten, M.T., 1980. A Closed-form Equation for Predicting the Hydraulic Conductivity of Unsaturated Soils. Soil Sci. Soc. Am. J. 44, 892–898. https://doi.org/10.2136/sssaj1980.03615995004400050002x

Venkatarama Reddy, B. V., Jagadish, K.S., 1993. The static compaction of soils. Geotechnique 43, 337–341. https://doi.org/10.1680/geot.1993.43.2.337

Villibor, D.F., Nogami, J.S., 2009. Economic Pavements - Technology for the use of fine laterite soils (in portuguese).

Wang, J.-D., Li, P., Ma, Y., Vanapalli, S.K., 2019. Evolution of pore-size distribution of intact loess and remolded loess due to consolidation. J. Soils Sediments 19, 1226–1238. https://doi.org/10.1007/s11368-018-2136-7

Wang, J.D., Li, P., Ma, Y., Vanapalli, S.K., Wang, X.G., 2020. Change in pore-size distribution of collapsible loess due to loading and inundating. Acta Geotech. 15, 1081–1094. https://doi.org/10.1007/s11440-019-00815-9

Wheeler, S.J., Sivakumar, V., 1995. An elasto-plastic critical state framework for unsaturated

853 soil. Geotechnique 45, 35–53. https://doi.org/10.1680/geot.1995.45.1.35

854 Yu, C.Y., Chow, J.K., Wang, Y.H., 2016. Pore-size changes and responses of kaolinite with
855 different structures subject to consolidation and shearing. Eng. Geol. 202, 122–131.
856 https://doi.org/10.1016/j.enggeo.2016.01.007

857

Declaration of interests

☒ The authors declare that they have no known competing financial interests or personal relationships that could have appeared to influence the work reported in this paper.

☐The authors declare the following financial interests/personal relationships which may be considered as potential competing interests:

CRediT Author statement

Vinícius de Oliveira Kühn: Conceptualization, Methodology, Validation, Formal analysis, Investigation, Data Curation, Writing - Original Draft, Review & Editing, Visualization.

Bruna de Carvalho Faria Lima Lopes: Conceptualization, Validation, Writing - Review & Editing, Visualization.

Bernardo Caicedo: Resources, Funding acquisition, Writing - Review & Editing.

Manoel Porfírio Cordão Neto: Resources, Funding acquisition, Writing - Review & Editing, Supervision, Project administration.